

Likelihood-Free Inference with Generative Neural Networks via Scoring Rule Minimization

Lorenzo Pacchiardi^{1*}, Ritabrata Dutta²

¹*Department of Statistics, University of Oxford, UK*

²*Department of Statistics, University of Warwick, UK*

Abstract

Bayesian Likelihood-Free Inference methods yield posterior approximations for simulator models with intractable likelihood. Recently, many works trained neural networks to approximate either the intractable likelihood or the posterior directly. Most proposals use normalizing flows, namely neural networks parametrizing invertible maps used to transform samples from an underlying base measure; the probability density of the transformed samples is then accessible and the normalizing flow can be trained via maximum likelihood on simulated parameter-observation pairs. A recent work [Ramesh et al., 2022] approximated instead the posterior with generative networks, which drop the invertibility requirement and are thus a more flexible class of distributions scaling to high-dimensional and structured data. However, generative networks only allow sampling from the parametrized distribution; for this reason, Ramesh et al. [2022] follows the common solution of adversarial training, where the generative network plays a min-max game against a “critic” network. This procedure is unstable and can lead to a learned distribution underestimating the uncertainty - in extreme cases collapsing to a single point. Here, we propose to approximate the posterior with generative networks trained by Scoring Rule minimization, an overlooked adversarial-free method enabling smooth training and better uncertainty quantification. In simulation studies, the Scoring Rule approach yields better performances with shorter training time with respect to the adversarial framework.

1 Introduction

Intractable-likelihood models are models for which it is impossible to evaluate the likelihood $p(\mathbf{y}|\boldsymbol{\theta})$ for an observation \mathbf{y} , but from which it is easy to simulate for any parameter value $\boldsymbol{\theta}$. Given \mathbf{y} and a prior $\pi(\boldsymbol{\theta})$, the standard Bayesian posterior is $\pi(\boldsymbol{\theta}|\mathbf{y}) \propto \pi(\boldsymbol{\theta})p(\mathbf{y}|\boldsymbol{\theta})$. However, obtaining that explicitly or sampling from it with Markov Chain Monte Carlo (MCMC) is impossible without having access to the likelihood.

Likelihood-Free Inference (LFI) techniques exploit model simulations to approximate the exact posterior distribution when the likelihood is unavailable. Popular approaches include Approximate Bayesian Computation methods [Lintusaari et al., 2017, Bernton et al., 2019] and Synthetic Likelihood [Price et al., 2018, An et al., 2020].

A recent strand of literature [Papamakarios and Murray, 2016, Lueckmann et al., 2017, Papamakarios et al., 2019, Lueckmann et al., 2019, Greenberg et al., 2019, Durkan et al., 2020, Radev et al., 2020] has explored using neural networks to perform LFI¹. Many methods employ normalizing flows [Papamakarios et al., 2021]: invertible neural networks which parametrize complex probability distributions by transforming a simple one (say, multivariate Gaussian). Normalizing flows allow direct sampling from the parametrized distribution and explicit density evaluation via the change-of-variables formula enabled by invertibility; using the latter, normalizing flows can be trained via maximum likelihood estimation on parameter-simulation pairs. They can be used to represent either the likelihood [Papamakarios et al., 2019, Lueckmann et al., 2019] or the posterior [Papamakarios and Murray, 2016, Lueckmann et al., 2017, Greenberg et al., 2019, Radev et al., 2020].

*Corresponding author: lorenzo.pacchiardi@stats.ox.ac.uk.

¹Check this website for an interactive up-to-date list.

However, requiring invertibility strongly constrains the network architecture. More general generative networks drop this requirement, thus gaining expressiveness and the ability to easily scale to large input and output sizes, but forgoing density evaluation: from a generative network, you can only obtain draws from the parametrized probability distribution. For this reason, maximum likelihood estimation of neural network weights is impossible and people use training methods based on generating samples from the generative network. A paradigmatic example is the popular Generative Adversarial Network, or GAN, framework of Goodfellow et al., 2014, where the generative network is trained in a min-max game against an additional *discriminator* network aiming at distinguishing between training samples and simulations from the generative network².

For LFI, Ramesh et al. [2022] used a generative network to represent a posterior approximation and trained it with an adversarial approach. From the trained network, approximate posterior samples can be directly obtained. Here, we build on Ramesh et al. [2022] by proposing a different training strategy based on minimizing values of Scoring Rules (SR, Gneiting and Raftery, 2007), which are functions assessing the match between a probability distribution and an observation. In contrast to the adversarial approach, plagued by biased gradient estimates [Bińkowski et al., 2018] and often leading to mode collapse (in which the parametrized probability distribution collapses on a single point, Richardson and Weiss, 2018), SR training has been found to better capture the full shape of the probability distribution in the setting of probabilistic forecasting [Pacchiardi et al., 2022]. Additionally, the SR-minimization approach leads to simpler training with respect to the adversarial one, as it does not require a discriminator or solving a min-max problem.

The rest of the paper is organized as follows. Section 2 discusses how to use a generative network to represent and approximate posterior and reviews the training method employed in Ramesh et al. [2022]. Section 3 we introduce the SR-minimization training for LFI. Section 4 reports simulation results and Section 5 gives concluding remarks.

Notation We will denote respectively by $\mathcal{Y} \subseteq \mathbb{R}^d$ and $\Theta \subseteq \mathbb{R}^p$ the data and parameter space. We will use $P(\cdot|\boldsymbol{\theta})$ and $p(\cdot|\boldsymbol{\theta})$ to denote the distribution and likelihood (with respect to Lebesgue measure) of the considered likelihood-free model. Π and π will denote prior distribution and prior density on Θ , and $\Pi(\cdot|\mathbf{y})$ and $\pi(\cdot|\mathbf{y})$ will denote corresponding posterior quantities for observation \mathbf{y} . In general, we will use P or Q to denote distributions, while S will denote a generic Scoring Rule. Other upper-case letters (\mathbf{X}, \mathbf{Y} and \mathbf{Z}) will denote random variables while lower-case ones will denote observed (fixed) values. We will denote by \mathbf{Y} or \mathbf{y} the observations (correspondingly random variables and realizations). Bold symbols denote vectors, and subscripts to bold symbols denote sample index (for instance, \mathbf{y}_i). Instead, subscripts to normal symbols denote component indices (for instance, y_j is the j -th component of \mathbf{y} , and $y_{i,j}$ is the j -th component of \mathbf{y}_i). Finally, \perp will denote independence between random variables, while $\mathbf{Y} \sim P$ indicates a random variable distributed according to P and $\mathbf{y} \sim P$ a sample from such random variable.

2 Approximate posterior via generative network

We use a generative network to represent an approximate posterior distribution $Q_\phi(\cdot|\mathbf{y})$ on the parameter space Θ given an observation $\mathbf{y} \in \mathcal{Y}$. The density of $Q_\phi(\cdot|\mathbf{y})$ (with respect to the Lebesgue measure) will be denoted by $q_\phi(\cdot|\mathbf{y})$. The generative network is defined via a neural network $g_\phi: \mathcal{Z} \times \mathcal{Y} \rightarrow \Theta$ transforming samples from a probability distribution $P_{\mathbf{z}}$ over the space \mathcal{Z} conditionally on an observation $\mathbf{y} \in \mathcal{Y}$; ϕ represents neural network weights. Samples from $Q_\phi(\cdot|\mathbf{y})$ are therefore obtained by sampling $\mathbf{z} \sim P_{\mathbf{z}}$ and computing $\boldsymbol{\theta} = g_\phi(\mathbf{z}, \mathbf{y}) \sim Q_\phi(\cdot|\mathbf{y})$ ³

In the following, as it is standard in the LFI setup, we assume to have access to parameter-simulations pairs $(\boldsymbol{\theta}_i, \mathbf{y}_i)_{i=1}^n$ generated from the prior $\boldsymbol{\theta}_i \sim \Pi$ and the model $\mathbf{y}_i \sim P(\cdot|\boldsymbol{\theta}_i)$; critically, these can also be considered as being samples from the data marginal $\mathbf{y}_i \sim P$ and the posterior

²Notice that generative networks and adversarial training are older techniques than normalizing flows. We introduce them in this order by following their usage in the LFI context.

³Formally, $Q_\phi(\cdot|\mathbf{y})$ is the push-forward of $P_{\mathbf{z}}$ through the map $g_\phi(\cdot, \mathbf{y}): Q_\phi(\cdot|\mathbf{y}) = g_\phi(\cdot, \mathbf{y})\#P_{\mathbf{z}}$, which means that, for any set A belonging to the Borel σ -algebra $\sigma(\Theta)$, $Q_\phi(A|\mathbf{y}) = P_{\mathbf{z}}(\{\mathbf{z} \in \mathcal{Z} : g_\phi(\mathbf{z}, \mathbf{y}) \in A\})$.

$\theta_i \sim \Pi(\cdot|\mathbf{y}_i)$. Using these samples, we want to tune ϕ such that $Q_\phi(\cdot|\mathbf{y}) \approx \Pi(\cdot|\mathbf{y})$ for all values of \mathbf{y} ; this is therefore an *amortized* setting [Radev et al., 2020], i.e. simulations from the likelihood-free models are drawn independently from the observations on which inference is required. We discuss strategies for tailoring simulations to a specific observation in Sec 3.4.

2.1 Adversarial posterior inference

In Ramesh et al. [2022], the posterior approximation Q_ϕ is trained in an adversarial framework. This requires introducing a *discriminator* or *critic* neural network $c_\psi : \Theta \times \mathcal{Y} \rightarrow \mathbb{R}$ with weights ψ whose task is to distinguish draws from the approximate and true posteriors. The loss employed in Ramesh et al. [2022] is the conditional version of the original GAN loss from Goodfellow et al. [2014], which was originally discussed in Mirza and Osindero [2014]:

$$\begin{aligned} L(\phi, \psi) &= \mathbb{E}_{\theta \sim \Pi} \mathbb{E}_{\mathbf{Y} \sim P(\cdot|\theta)} \mathbb{E}_{\mathbf{Z} \sim P_{\mathbf{Z}}} [\log c_\psi(\theta, \mathbf{Y}) + \log(1 - c_\psi(g_\phi(\mathbf{Z}, \mathbf{Y}), \mathbf{Y}))] \\ &= \mathbb{E}_{\mathbf{Y} \sim P} \left[\mathbb{E}_{\theta \sim \Pi(\cdot|\mathbf{Y})} (\log c_\psi(\theta, \mathbf{Y})) + \mathbb{E}_{\tilde{\theta} \sim Q_\phi(\cdot|\mathbf{Y})} \left(\log \left(1 - c_\psi(\tilde{\theta}, \mathbf{Y}) \right) \right) \right], \end{aligned} \quad (1)$$

whose saddle point solution

$$\min_{\phi} \max_{\psi} L(\phi, \psi) \quad (2)$$

leads to $Q_\phi(\cdot|\mathbf{y})$ being the exact posterior for all choices of \mathbf{y} for which $p(\mathbf{y}) > 0$ (provided q_ϕ and c_ψ have infinite expressive power; that in fact corresponds to minimizing the Jensen-Shannon divergence, see Appendix A for more details).

In practice, the training procedure works by Stochastic Gradient Descent (SGD): we replace the expectations in Eq. (2.1) with empirical means over (a mini-batch of) the training dataset and draws from the generative network and alternate maximization steps over ψ with minimization steps over ϕ . This alternating optimization is however unstable and requires careful hyperparameters tuning and specialized training routines; additionally, doing a finite number of maximization steps over ψ and then using the current value of ψ to compute gradients of the objective with respect to ϕ leads to biased gradient estimates Bińkowski et al. [2018]. A possible consequence of this is mode collapse Richardson and Weiss [2018], in which the distribution parametrized by the generative network collapses onto a single point. This may not be an issue in some applications of generative networks where uncertainty quantification is not important, but it can be detrimental for approximate posterior inference.

3 Posterior inference via Scoring Rules minimization

We discuss here how to use Scoring Rules to define an adversarial-free training objective for generative networks, focusing on the specific case of a generative network parametrizing an approximate posterior. In Pacchiardi et al. [2022], more details on SR-training and its application to probabilistic forecasting can be found. Other works employing SR training, albeit not for the LFI framework, are Bouchacourt et al. [2016], Gritsenko et al. [2020], Harakeh and Waslander [2021].

3.1 Scoring Rule training

We first introduce Scoring Rules for a distribution P related to a generic random variable \mathbf{X} . A Scoring Rule (SR, Gneiting and Raftery, 2007) $S(P, \mathbf{x})$ is a function of P and of an observation \mathbf{x} of the random variable \mathbf{X} . If \mathbf{X} is actually distributed according to Q , the expected Scoring Rule is defined as:

$$S(P, Q) := \mathbb{E}_{\mathbf{X} \sim Q} S(P, \mathbf{X}),$$

The Scoring Rule S is *proper* relative to a set of distributions \mathcal{P} over \mathcal{X} if

$$S(Q, Q) \leq S(P, Q) \quad \forall P, Q \in \mathcal{P},$$

i.e., if the expected Scoring Rule is minimized in P when $P = Q$. Moreover, S is *strictly proper* relative to \mathcal{P} if $P = Q$ is the unique minimum:

$$S(Q, Q) < S(P, Q) \quad \forall P, Q \in \mathcal{P} \text{ s.t. } P \neq Q.$$

Let us now go back to the Bayesian LFI setting introduced at the start of the paper. Denoting by $Q_\phi(\cdot|\mathbf{y})$ the approximate posterior parametrized by the generative network, solving the following problem for a strictly proper S :

$$\arg \min_{\phi} \mathbb{E}_{\mathbf{Y} \sim P} \mathbb{E}_{\boldsymbol{\theta} \sim \Pi(\cdot|\mathbf{Y})} S(Q_\phi(\cdot|\mathbf{Y}), \boldsymbol{\theta}) = \arg \min_{\phi} \mathbb{E}_{\boldsymbol{\theta} \sim \Pi} \mathbb{E}_{\mathbf{Y} \sim P(\cdot|\boldsymbol{\theta})} S(Q_\phi(\cdot|\mathbf{Y}), \boldsymbol{\theta}) \quad (3)$$

leads to $q_\phi(\cdot|\mathbf{y}) = \pi(\cdot|\mathbf{y})$ for all values of \mathbf{y} for which $p(\mathbf{y}) > 0$.

Replacing the expectations in Eq. (3.1) with empirical means over the training dataset yields:

$$\arg \min_{\phi} \frac{1}{n} \sum_{i=1}^n S(Q_\phi(\cdot|\mathbf{y}_i), \boldsymbol{\theta}_i); \quad (4)$$

computing the objective directly is intractable as, in general, we do not have access to $S(Q_\phi(\cdot|\mathbf{y}), \boldsymbol{\theta})$. Notice, however, that in order to train Q_ϕ via SGD it is enough to obtain unbiased estimates of $\nabla_{\phi} S(Q_\phi(\cdot|\mathbf{y}_i), \boldsymbol{\theta}_i)$, which can be easily done whenever S admits an easy unbiased empirical estimator \hat{S} , i.e. such that:

$$\mathbb{E} \left[\hat{S}(\{\tilde{\boldsymbol{\theta}}_j^{(\mathbf{y})}\}_{j=1}^m, \boldsymbol{\theta}) \right] = S(Q_\phi(\cdot|\mathbf{y}), \boldsymbol{\theta}),$$

where the expectation is over $\tilde{\boldsymbol{\theta}}_j^{(\mathbf{y})} \sim Q_\phi(\cdot|\mathbf{y})$. More details can be found in Appendix B.2. If S admits such an estimator, each step of SGD involves generating m simulations from the generative network $Q_\phi(\cdot|\mathbf{y}_i)$ for each \mathbf{y}_i in the training batch.

Below, we introduce some SRs for which easy unbiased estimators of the form above are available. These estimators however require $m > 1$; to train GAN, instead, a single draw from the generative network was enough. In experiments, however, small values of m ($m = 10$ for instance) lead to satisfactory results. Additionally, as mentioned above, the SR approach does not require a discriminator network and has a smoother training process, which implies convergence is generally reached with less training epochs. These two factors lead to lower computational and memory cost with respect to adversarial training (see Section 4 for details).

3.2 Some Scoring Rules with unbiased estimators

We introduce two specific Scoring Rules that we use in our experiments, by considering again a generic distribution P and random variable \mathbf{X} .

Energy score The energy score⁴. is given by:

$$S_E^{(\beta)}(P, \mathbf{x}) = 2 \cdot \mathbb{E} \left[\|\tilde{\mathbf{X}} - \mathbf{x}\|_2^\beta \right] - \mathbb{E} \left[\|\tilde{\mathbf{X}} - \tilde{\mathbf{X}}'\|_2^\beta \right], \quad \tilde{\mathbf{X}} \perp \tilde{\mathbf{X}}' \sim P, \quad (5)$$

where $\beta \in (0, 2)$. This is a strictly proper SR for the class of probability measures P such that $\mathbb{E}_{\tilde{\mathbf{X}} \sim P} \|\tilde{\mathbf{X}}\|^\beta < \infty$ [Gneiting and Raftery, 2007]. An unbiased estimate can be obtained by replacing the expectations in $S_E^{(\beta)}$ with empirical means over draws from P (see Appendix B.1) We will fix $\beta = 1$ in the rest of this work.

Kernel score When $k(\cdot, \cdot)$ is a positive definite kernel, the kernel score for k can be defined as [Gneiting and Raftery, 2007]:

$$S_k(P, \mathbf{x}) = \mathbb{E}[k(\tilde{\mathbf{X}}, \tilde{\mathbf{X}}')] - 2 \cdot \mathbb{E}[k(\tilde{\mathbf{X}}, \mathbf{x})], \quad \tilde{\mathbf{X}} \perp \tilde{\mathbf{X}}' \sim P. \quad (6)$$

The kernel score is proper for the class of probability distributions P for which $\mathbb{E}_{\tilde{\mathbf{X}}, \tilde{\mathbf{X}}' \sim P} [k(\tilde{\mathbf{X}}, \tilde{\mathbf{X}}')]$ is finite (by Theorem 4 in Gneiting and Raftery [2007]). It is closely related to the kernel Maximum

⁴The probabilistic forecasting literature [Gneiting and Raftery, 2007] use a different convention for the energy score and the subsequent kernel score, which amounts to multiplying our definitions by 1/2. We follow here the convention used in the statistical inference literature [Rizzo and Székely, 2016, Chérif-Abdellatif and Alquier, 2020, Nguyen et al., 2020]

Mean Discrepancy (MMD, Gretton et al., 2012) and is strictly proper under conditions ensuring the MMD is a metric [Gretton et al., 2012]. These conditions are satisfied, among others, by the Gaussian kernel (which we will use in this work):

$$k(\tilde{\mathbf{x}}, \mathbf{x}) = \exp\left(-\frac{\|\tilde{\mathbf{x}} - \mathbf{x}\|_2^2}{2\gamma^2}\right),$$

in which γ is a scalar bandwidth. As for the Energy Score, an unbiased estimate can be obtained by replacing the expectations in S_k with empirical means over draws from P (see Appendix B.1).

Patched SR We now discuss a way to build a composite SR which encodes structural information in \mathbf{X} . In fact, if \mathbf{X} has some structure (say, it is on a 1D or 2D grid), computing the raw SRs above discards that information. A way to encode some of it is to compute the SRs on localized *patches* across the grid and cumulate the score; in this way, short-scale correlations are given more importance. However, the resulting Scoring Rule is not strictly proper; to fix this, we add the SR computed over the full \mathbf{x} , which makes the overall SR strictly proper (see Lemma 3.4 in Pacchiardi et al. [2022]).

For a given SR S , therefore, the patched SR is:

$$S_p(P, \mathbf{x}) = w_1 S(P, \mathbf{x}) + w_2 \sum_{p \in \mathcal{P}} S(P|_p, \mathbf{x}|_p),$$

where $w_1, w_2 > 0$, $|_p$ denotes the restriction of a distribution or of a vector to a patch p and \mathcal{P} is a set of patches. See Pacchiardi et al. [2022] for more discussion on patched SRs.

3.3 Connection with normalizing flows

As mentioned in the introduction, normalizing flows are generative networks which impose invertibility of the map $g_\phi(\mathbf{z}, \mathbf{y})$ with respect to \mathbf{z} . As such, density evaluation of the resulting q_ϕ is possible via the change-of-variables formula, so that ϕ is usually trained via maximum likelihood [Papamakarios et al., 2021]. For instance, in Radev et al. [2020], the following problem is considered, where \mathbb{KL} denotes the Kullback-Leibler divergence:

$$\begin{aligned} & \underset{\phi}{\operatorname{argmin}} \mathbb{E}_{\mathbf{Y} \sim P} [\mathbb{KL}(\Pi(\cdot | \mathbf{Y}) \| Q_\phi(\cdot | \mathbf{Y}))] \\ &= \underset{\phi}{\operatorname{argmin}} \mathbb{E}_{\mathbf{Y} \sim P} \mathbb{E}_{\boldsymbol{\theta} \sim \Pi(\cdot | \mathbf{Y})} [-\log q_\phi(\boldsymbol{\theta} | \mathbf{Y})] \\ &= \underset{\phi}{\operatorname{argmin}} \mathbb{E}_{\boldsymbol{\theta} \sim \Pi} \mathbb{E}_{\mathbf{Y} \sim P(\cdot | \boldsymbol{\theta})} [-\log q_\phi(\boldsymbol{\theta} | \mathbf{Y})], \end{aligned}$$

which corresponds to our SR-based approach in Eq. (3.1) by identifying $S(Q_\phi(\cdot | \mathbf{y}), \boldsymbol{\theta}) = -\log q_\phi(\boldsymbol{\theta} | \mathbf{y})$, which is the strictly-proper logarithmic scoring rule.

3.4 Sequential training

Up to this point, we have considered the training data from the simulator model $(\boldsymbol{\theta}_i, \mathbf{y}_i)_{i=1}^n$ to be generated independently from the observation on which inference is performed; under this assumption, we have discussed ways to learn posterior approximations valid for all values of \mathbf{y} such that $p(\mathbf{y}) > 0$. Once the neural network is trained, therefore, inference can be performed for as many observations as we wish. This is a so-called *amortized* setup Radev et al. [2020].

However, practitioners may require posterior inference for a single observation \mathbf{y}_o . What they are interested in, therefore, is the quality of the approximation for values of $\boldsymbol{\theta}$ at which the true posterior density is large for the observed \mathbf{y}_o . In this case, generating training samples independently from \mathbf{y}_o may be wasteful: a more efficient method (in terms of simulations from the model $p(\cdot | \boldsymbol{\theta})$) would generate training samples $\boldsymbol{\theta}_i$'s close to the modes of the true posterior. This can be done in a sequential fashion: given a small amount of training data, a first approximation Q_{ϕ_1} is obtained; from that, additional training samples $(\boldsymbol{\theta}_i, \mathbf{y}_i)$ are generated by $\boldsymbol{\theta}_i \sim Q_{\phi_1}(\cdot | \mathbf{y}_o)$, $\mathbf{y}_i \sim P(\cdot | \boldsymbol{\theta}_i)$ and used to (re-)train an approximation Q_{ϕ_2} . This procedure is iterated several times, allowing therefore the

training samples to progressively better cover the posterior modes, which in turn allows to refine the posterior approximation close to the modes [Lueckmann et al., 2017, Greenberg et al., 2019].

However, naively following that strategy is incorrect. To see this, assume that, at the second round, we just train on samples drawn from the approximate posterior $\tilde{\Pi} = Q_{\phi_1}(\cdot|\mathbf{y}_o)$ obtained at the first round. Such a sampled pair $(\boldsymbol{\theta}_i, \mathbf{y}_i)$ was drawn from a joint density $\tilde{\pi}(\boldsymbol{\theta}_i)p(\mathbf{y}_i|\boldsymbol{\theta}_i) = \tilde{p}(\mathbf{y}_i)\tilde{\pi}(\boldsymbol{\theta}_i|\mathbf{y}_i)$, where $\tilde{\pi}$ on the left-hand side of the equality is the density of the proposal $\tilde{\Pi}$ and the quantities on the right-hand side are univocally defined by the left-hand side. The optimal ϕ^* obtained via SR-minimization thus corresponds to $q_{\phi^*}(\cdot|\mathbf{y}) = \tilde{\pi}(\cdot|\mathbf{y})$, which is not the correct target.

The traditional way to fix this entails introducing importance weights in the training objective (Eq. 3.1):

$$\mathbb{E}_{\boldsymbol{\theta} \sim \Pi} \mathbb{E}_{\mathbf{Y} \sim P(\cdot|\boldsymbol{\theta})} S(Q_{\phi}(\cdot|\mathbf{Y}), \boldsymbol{\theta}) = \mathbb{E}_{\boldsymbol{\theta} \sim \tilde{\Pi}} \frac{\pi(\boldsymbol{\theta})}{\tilde{\pi}(\boldsymbol{\theta})} \mathbb{E}_{\mathbf{Y} \sim P(\cdot|\boldsymbol{\theta})} S(Q_{\phi}(\cdot|\mathbf{Y}), \boldsymbol{\theta}).$$

As $\tilde{\pi}(\boldsymbol{\theta})$ cannot be evaluated, a solution is to fit a probabilistic classifier (at each round of the sequential procedure) to samples from $\pi(\boldsymbol{\theta})$ and $\tilde{\pi}(\boldsymbol{\theta})$ and use it to estimate the ratio $\frac{\pi(\boldsymbol{\theta})}{\tilde{\pi}(\boldsymbol{\theta})}$. This classifier is not required for the normalizing flows approaches, where the ratio can be evaluated explicitly [Lueckmann et al., 2017, Greenberg et al., 2019] (unless the prior π is also defined implicitly, as in the camera model example in Section 4). For the GAN approach, a similar importance weights approach requires additionally to estimate the ratio $\frac{\tilde{p}(\mathbf{y})}{p(\mathbf{y})}$ [Ramesh et al., 2022].

An alternative approach, which was proposed in Ramesh et al. [2022], involves correcting the distribution of the variable \mathbf{Z} which is transformed by the generative network. Specifically, Ramesh et al. [2022] shows that $\pi(\boldsymbol{\theta}|\mathbf{y}) = \tilde{\pi}(\boldsymbol{\theta}|\mathbf{y})w(\boldsymbol{\theta}, \mathbf{y}) \iff \tilde{\pi}(\boldsymbol{\theta}|\mathbf{y}) = \pi(\boldsymbol{\theta}|\mathbf{y})(w(\boldsymbol{\theta}, \mathbf{y}))^{-1}$, where $w(\boldsymbol{\theta}, \mathbf{y}) = \frac{\pi(\boldsymbol{\theta})\tilde{p}(\mathbf{y})}{\tilde{\pi}(\boldsymbol{\theta})p(\mathbf{y})}$. Therefore you can consider a modified approximation $\tilde{Q}_{\phi}(\cdot|\mathbf{Y})$ and a new training objective:

$$\mathbb{E}_{\mathbf{Y} \sim \tilde{P}} \mathbb{E}_{\boldsymbol{\theta} \sim \tilde{\Pi}(\cdot|\mathbf{Y})} S(\tilde{Q}_{\phi}(\cdot|\mathbf{Y}), \boldsymbol{\theta}) = \mathbb{E}_{\boldsymbol{\theta} \sim \tilde{\Pi}} \mathbb{E}_{\mathbf{Y} \sim P(\cdot|\boldsymbol{\theta})} S(\tilde{Q}_{\phi}(\cdot|\mathbf{Y}), \boldsymbol{\theta}) \quad (7)$$

whose minimization leads to $\tilde{Q}_{\phi}(\cdot|\mathbf{Y}) = \tilde{\Pi}(\cdot|\mathbf{Y})$. By setting

$$\tilde{Q}_{\phi}(\cdot|\mathbf{Y}) = Q_{\phi}(\cdot|\mathbf{Y})(w(\boldsymbol{\theta}, \mathbf{y}))^{-1},$$

you ensure $Q_{\phi}(\cdot|\mathbf{Y}) = \Pi(\cdot|\mathbf{Y})$. To train ϕ using the objective in Eq. (3.4), draws from $\tilde{Q}_{\phi}(\cdot|\mathbf{Y})$ are required; those can be obtained by sampling $\mathbf{z} \sim \tilde{P}_{\mathbf{z}}$ where $\tilde{p}_{\mathbf{z}}(\mathbf{z}) = p_{\mathbf{z}}(\mathbf{z})(w(g_{\phi}(\mathbf{z}, \mathbf{y}), \mathbf{y}))^{-1}$ and then computing $\boldsymbol{\theta} = g_{\phi}(\mathbf{z}, \mathbf{y})$, which is thus a sample from $\tilde{Q}_{\phi}(\cdot|\mathbf{Y})$. Sampling from $\tilde{P}_{\mathbf{z}}$ entails either Rejection sampling or MCMC. Additionally, this method, this correction requires estimating two ratios via probabilistic classifiers ($\frac{\tilde{p}(\mathbf{y})}{p(\mathbf{y})}$ and $\frac{\pi(\boldsymbol{\theta})}{\tilde{\pi}(\boldsymbol{\theta})}$). The advantage with respect to the importance weight strategy is reduced variance of the training objective; however, a larger computational cost in obtaining the corrected samples from the latent distribution is involved (with repeated passes through the NNs approximating the ratios for each training sample \mathbf{y}_i). The strategy discussed above can seamlessly be applied in the GAN approach as well [Ramesh et al., 2022].

On the considered examples in Ramesh et al. [2022], the sequential approaches did not provide any advantage with respect to the amortized ones, mainly due to the additional computational cost associated to estimating the ratios. As we use the same examples here, we do not test these methods, but we discussed them anyway as they may turn out to be useful in other applications.

4 Simulation study

Following Ramesh et al. [2022], we present here results on two benchmark problems and two high-dimensional models, one of which has an implicitly defined prior. For all examples, we evaluate the performance of the different methods as in Ramesh et al. [2022]. Besides that, we assess the calibration of the approximate posteriors by the discrepancy between credible intervals in the approximate posteriors and the frequency with which the true parameter belongs to the credible interval itself (we term this metric *calibration error*). We also evaluate how close the posterior means are to the true parameter value by the *Normalized Root Mean-Square Error* (NRMSE) and the *coefficient of determination* R^2 ; these metrics were used for LFI in Radev et al. [2020]; we provide more detail in

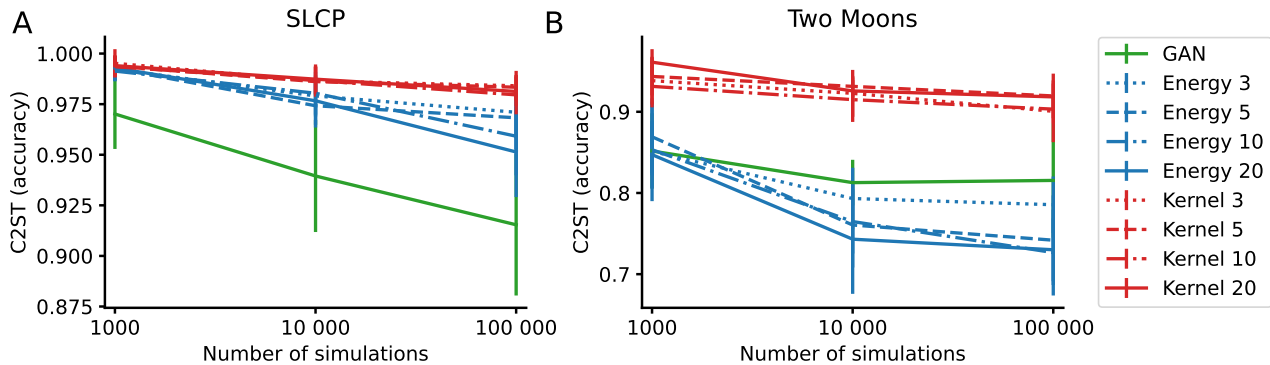


Figure 1: C2ST for SR and GAN methods for the SLCP and Two Moons benchmarks. For the SR methods, we report values for all numbers of generative network samples m used in training. SLCP: GAN performs better, but poorly on an absolute scale. Two Moons: methods based on the Energy Score perform better.

Appendix C. As all these metrics are for scalar variables, we compute their values independently for each component of θ and report their average.

We compare our generative networks trained with SRs with the GAN-based one in Ramesh et al. [2022]; in both setups, we adapt the generative networks defined in Ramesh et al. [2022] for the different tasks. Additional training details for all models are reported in Appendix D. Notice how Ramesh et al. [2022] compared with additional LFI methods, concluding that the generative-network based one performs worse for the simple models but is competitive for the high-dimensional ones. Here, we do not compare with these other methods as the focus of our paper is to provide a different training strategy for the generative-network based one, for which the adversarial strategy was previously the only option.

4.1 Benchmark models

We consider here the “Simple Likelihood Complex Posterior” (SLCP) and the “Two Moons” benchmarks; in the former, a 5-dimensional θ defines the distribution of an 8-dimensional Gaussian \mathbf{y} in a nonlinear manner. In the Two Moons model, both \mathbf{y} and θ are 2-dimensional. We refer to Ramesh et al. [2022] and references therein for more details⁵ For both models, we train all methods on $n_{\text{train}} = 1000, 10000$ and 100000 posterior samples. We consider the SR methods with the Energy and Kernel Score trained with $m = 3, 5, 10$ or 20 samples from the generative network for each \mathbf{y}_i in a training batch. The SR methods are trained on a single CPU, while GAN is trained on an NVIDIA Tesla-V100 GPU. For the Two Moons model, we do not use early stopping for the SR methods; additionally, we employ the optimal configuration found in Ramesh et al. [2022] for GAN.

For these two models, samples from reference posteriors are available [Lueckmann et al., 2021]; therefore, as done in Ramesh et al. [2022], we assess the performance of the different methods via the discrimination ability of a classifier trained to distinguish samples from the reference and approximate posteriors (classification-based two-sample test, C2ST). If the classification accuracy is 0.5, the classifier is unable to distinguish between the two sets of samples, implying perfect posterior approximation.

In Figure 1, we report C2ST values for the GAN and SR methods for the different number of training simulations. For SLCP, GAN performs better (although the performance is poor on an absolute scale and worse than other LFI methods, see Ramesh et al., 2022). For the Two Moons method, methods based on the Energy Score perform better.

In Tables 1 and 2, we report other performance metrics, together with the runtime and the epoch at which training was early stopped, for GAN, Energy and Kernel Score, with $n_{\text{train}} = 100000$ and $m = 20$. Notice how the SR methods were trained in much shorter time (and on a single CPU). Additional results are reported in Appendices E.1 and E.2.

⁵These models are implemented in the `sbibm` Python package, whose accompanying paper Lueckmann et al. [2021] provides additional details.

Table 1: SLCP: performance metrics, runtime and early stopping epoch for GAN, Energy and Kernel Score methods, with $n_{\text{train}} = 100000$ and $m = 20$. Notice how the SR methods were trained on a single CPU, while GAN was trained on a GPU. The maximum number of training epochs was 20000.

	C2ST ↓	NRMSE ↓	Cal. Err. ↓	R^2 ↑	Runtime (sec)	Early stopping epoch
GAN	0.92 ± 0.03	0.23 ± 0.05	0.06 ± 0.03	0.35 ± 0.30	30963	20000
Energy	0.95 ± 0.02	0.22 ± 0.06	0.07 ± 0.04	0.38 ± 0.32	1645	2100
Kernel	0.98 ± 0.01	0.22 ± 0.06	0.13 ± 0.10	0.37 ± 0.31	1210	1200

Table 2: Two Moons: performance metrics, runtime and early stopping epoch for GAN, Energy and Kernel Score methods, with $n_{\text{train}} = 100000$ and $m = 20$. Notice how the SR methods were trained on a single CPU, while GAN was trained on a GPU. Here, no early stopping was used (the maximum number of training epochs was 20000).

	C2ST ↓	NRMSE ↓	Cal. Err. ↓	R^2 ↑	Runtime (sec)	Early stopping epoch
GAN	0.82 ± 0.07	0.20 ± 0.00	0.07 ± 0.02	0.51 ± 0.01	30232	20000
Energy	0.73 ± 0.04	0.20 ± 0.00	0.03 ± 0.00	0.51 ± 0.01	10805	20000
Kernel	0.92 ± 0.02	0.20 ± 0.00	0.03 ± 0.01	0.50 ± 0.01	10902	20000

4.2 Shallow water model

The shallow water model is obtained as the discretization of a PDE describing the propagation of an initial disturbance across the surface of a shallow basin; the parameter $\theta \in \mathbb{R}^{100}$ represents the depth of the basin at equidistant points; the simulator outputs the evolution over 100 time-steps (producing a raw observation of size $100 \times 100 = 10000$); then, a Fourier transform is computed and the real and imaginary parts are concatenated and summed to Gaussian noise, leading to $\mathbf{y} \in \mathbb{R}^{20k}$. More details are given in Ramesh et al. [2022]. Besides the GAN method, we test here the Energy and Kernel score with $m = 10$ computed in three different configurations: 1) on the full parameter space, 2) with patch size 10 and step 5, and 3) with patch size 20 and step 10. Training is done on 100k samples on a NVIDIA Tesla-V100 GPU; additional details are discussed in Appendix D.2. Among the SR methods, the Energy Score with patch size 20 and step 10 performed better; therefore, we report only results for that method in the main body of the paper; results for the other configurations are given in Appendix E.3.

In Figure 2, we report posterior and posterior predictive samples for both methods, together with prior samples and the ground-truth depth profile. For the Energy Score, posterior samples better follow the ground truth profile and, similarly, posterior predictive samples better match the true observation.

In Table 3, we report the performance metrics, runtime and epoch of early stopping of the GAN and Energy Score method; notice how the calibration error is much smaller for the latter, which was additionally trained in much shorter time. We also assess calibration via Simulation Based Calibration (Talts et al., 2018, details in Appendix C.2.2) in Figure 3. That as well highlights how the calibration of the Energy Score method is better than the one achieved by GAN.

4.3 Noisy Camera model

Here, we consider $\theta \in \mathbb{R}^{28 \times 28}$ to be the images of the EMNIST dataset [Cohen et al., 2017], from which the data $\mathbf{y} \in \mathbb{R}^{28 \times 28}$ is generated by applying some blurring (see Ramesh et al., 2022 for details). Posterior inference corresponds therefore to Bayesian denoising. In this model, the dimension of parameter space is larger than in typical LFI applications; additionally, the prior is defined implicitly as we can only generate samples from it. This prevents the application of most standard LFI methods. Besides the GAN method, we test here the Energy and Kernel score with $m = 10$ in three

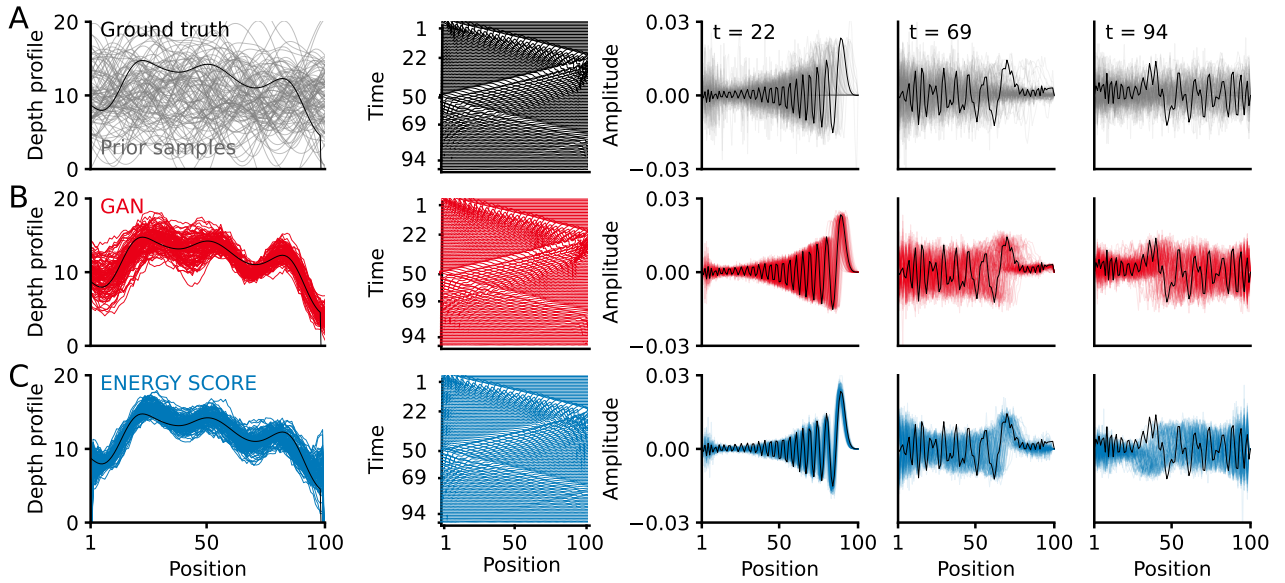
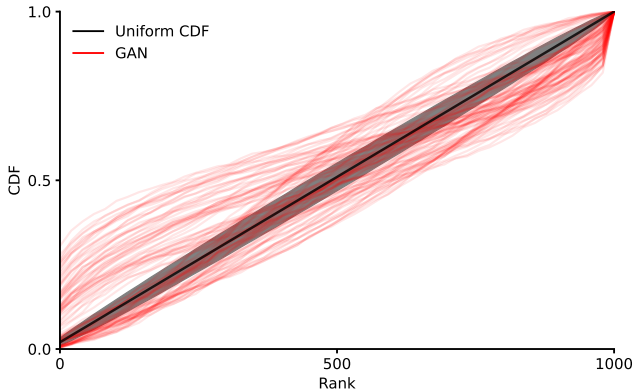


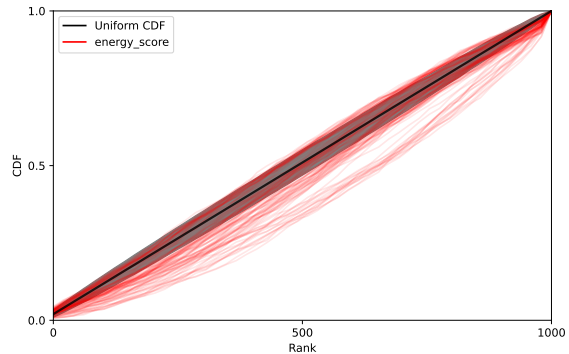
Figure 2: Shallow water model: inference results with GAN and Energy Score with patch size 20 and step 10. The figure structure closely follows that in Ramesh et al. [2022]. Row A: Ground truth, observation and prior samples. Left: ground-truth depth profile and prior samples. Middle: surface wave simulated from ground-truth profile as a function of position and time. Right: wave amplitudes at three different fixed times for ground-truth depth profile (black), and waves simulated from multiple prior samples (gray). Rows B and C refer respectively to GAN and Energy Score (with patch size 20 and step 10). For both, left represents posterior samples versus ground-truth depth profile (black), from which it can be seen how posterior samples for the Energy Score better follow the truth with respect to GAN; middle represents surface wave simulated from a single posterior sample; right represents wave amplitudes simulated from multiple posterior samples, at three different fixed times, with black line denoting the actual observation; again, Energy Score better follows the observation, except for $t = 94$.

Table 3: Shallow Water model: performance metrics, runtime and early stopping epoch for GAN and the Energy Score with patch size 20 and step 10. The latter method achieved better results with shorter training time. We do not train GAN from scratch but rather relied on the trained network obtained in Ramesh et al. [2022]. The training time we report here corresponds to what is mentioned in Ramesh et al. [2022], which used two GPUs for training (with respect to a single one for the SR methods). For the same reason, we do not report the epoch at which GAN training was early stopped.

	NRMSE ↓	Cal. Err. ↓	R ² ↑	Runtime (sec)	Early stopping epoch
Energy	0.05 ± 0.01	0.03 ± 0.02	0.89 ± 0.05	60017	12400
GAN	0.07 ± 0.01	0.12 ± 0.09	0.78 ± 0.05	≈345600	-



(a) GAN



(b) Energy Score, patch size 20 and step 10

Figure 3: Shallow Water model: Simulation Based Calibration. Each line corresponds to a single dimension of θ and represents the CDF of the rank of the true parameter value with respect to a set of posterior samples. A calibrated posterior implies uniform CDF (diagonal black line, with associated 99% confidence region for that number of samples in gray).

different configurations: 1) on the full parameter space, 2) with patch size 14 and step 7, and 3) with patch size 8 and step 5. Training is done on 800 thousands samples on a NVIDIA Tesla-V100 GPU; additional details are discussed in Appendix D.3. Among the SR methods, those with patch size 8 and step 5 performed better; therefore, we report only results for the Kernel and Energy Score in that configuration in the main body of the paper; results for the other configurations are given in Appendix E.4.

In Figure 4, we report posterior mean and standard deviation for a set of observations for the different methods. SR methods lead to cleaner image reconstruction and more meaningful uncertainty quantification.

In Table 4, we report the performance metrics, runtime and epoch of early stopping of the GAN and SR methods; the latter lead to smaller calibration error, although that is still quite poor in absolute terms. The R² values here are also poor. We believe these low metric values are due to each pixel only taking a discrete set of values between 0 and 1, with white spaces assigned 0 and darkest pixels being assigned 1. The generative network outputs is also bounded in (0, 1) but can never reach 0 or 1 as it is obtained via a continuous transformation from \mathbb{R} . For the calibration error (see Appendix C.2.1), that means that a credible interval obtained from the generative network cannot contain the extreme values 0 or 1; similarly, the approximate posterior mean can never be smaller than 0 or larger than 1, thus decreasing the R² values (see Appendix C.1.2). Additionally, we report here the un-normalized RMSE, as computing the normalization would lead to infinite values for the pixels in which the true value is 0 for all training samples (see Appendix C.1.1).



Figure 4: Noisy Camera model: ground truth and posterior inference with different methods, for a set of observations (each observation corresponds to a column). The first two rows represent the ground-truth values of θ and the corresponding observation y_o . The remaining rows represent mean and Standard Deviation (SD) for GAN and Energy and Kernel Score methods with patch size 8 and step 5. Notice how the posterior mean for the SR methods are neater than those obtained with GAN; additionally, the SD is larger close to the boundary of the reconstructed digit (notice the different color scale in the SD for GAN and for the SR methods).

5 Conclusions

We considered using a generative network to represent posterior distributions for Likelihood-Free Inference, following Ramesh et al. [2022], and investigated training it via Scoring Rule minimization rather than in an adversarial setup as was done in Ramesh et al. [2022]. The Scoring Rule approach is theoretically grounded and does not suffer from training instability and biased gradients, as the adversarial approach does. In simulation studies, and especially on high-dimensional tasks, we found the Scoring Rule approach generally performed better and was substantially cheaper to train. These findings corroborate similar ones reported in Pacchiardi et al. [2022] in the setting of probabilistic forecasting, making Scoring Rules minimization an appealing method to train generative networks, particularly when uncertainty quantification in the approximate distribution is critical.

In our simulation studies, we only considered the original GAN objective [Goodfellow et al., 2014] in the adversarial setup, which is what Ramesh et al. [2022] did. We believe more advanced adversarial training would lead to better results; however, in Pacchiardi et al. [2022], Scoring Rule minimization

Table 4: Noisy Camera model: performance metrics, runtime and early stopping epoch for GAN and for the Energy and Kernel Score with patch size 8 and step 5. The latter methods achieved better performance with shorter training time. All methods are trained on a single GPU.

	RMSE ↓	Cal. Err. ↓	R ² ↑	Runtime (sec)	Early stopping epoch
GAN	0.25 ± 0.19	0.50 ± 0.00	-23.94 ± 366.08	45398	3600
Energy	0.06 ± 0.05	0.36 ± 0.12	-2.14 ± 55.86	22633	4000
Kernel	0.07 ± 0.05	0.36 ± 0.12	-10.29 ± 222.12	22545	3200

was shown to outperform even more advanced adversarial approaches for probabilistic forecasting, while still being cheaper and easier to train. We expect the same holds for Likelihood-Free Inference.

Acknowledgements

The authors thank Poornima Ramesh for help using the code used to create the results reported in Ramesh et al. [2022] and for providing additional result files.

LP is supported by the EPSRC and MRC through the OxWaSP CDT programme (EP/L016710/1), which also funds the computational resources used to perform this work. RD is funded by EPSRC (grant nos. EP/V025899/1, EP/T017112/1) and NERC (grant no. NE/T00973X/1). We thank Geoff Nicholls for valuable feedback and suggestions.

References

- Z. An, D. J. Nott, and C. Drovandi. Robust Bayesian synthetic likelihood via a semi-parametric approach. *Statistics and Computing*, 30(3):543–557, 2020.
- M. Arjovsky, S. Chintala, and L. Bottou. Wasserstein generative adversarial networks. In *International conference on machine learning*, pages 214–223. PMLR, 2017.
- E. Bernton, P. E. Jacob, M. Gerber, and C. P. Robert. Approximate Bayesian computation with the Wasserstein distance. *Journal of the Royal Statistical Society: Series B (Statistical Methodology)*, 81(2):235–269, 2019. doi: <https://doi.org/10.1111/rssb.12312>. URL <https://rss.onlinelibrary.wiley.com/doi/abs/10.1111/rssb.12312>.
- M. Bińkowski, D. J. Sutherland, M. Arbel, and A. Gretton. Demystifying MMD GANs. In *International Conference on Learning Representations*, 2018.
- D. Bouchacourt, P. K. Mudigonda, and S. Nowozin. DISCO nets: DISsimilarity COefficient networks. *Advances in Neural Information Processing Systems*, 29:352–360, 2016.
- B.-E. Chérif-Abdellatif and P. Alquier. MMD-Bayes: Robust Bayesian estimation via maximum mean discrepancy. In *Symposium on Advances in Approximate Bayesian Inference*, pages 1–21. PMLR, 2020.
- G. Cohen, S. Afshar, J. Tapson, and A. Van Schaik. EMNIST: Extending MNIST to handwritten letters. In *2017 international joint conference on neural networks (IJCNN)*, pages 2921–2926. IEEE, 2017.
- C. Durkan, I. Murray, and G. Papamakarios. On contrastive learning for likelihood-free inference. In *International Conference on Machine Learning*, pages 2771–2781. PMLR, 2020.
- T. Gneiting and A. E. Raftery. Strictly proper scoring rules, prediction, and estimation. *Journal of the American statistical Association*, 102(477):359–378, 2007.
- T. Gneiting, F. Balabdaoui, and A. E. Raftery. Probabilistic forecasts, calibration and sharpness. *Journal of the Royal Statistical Society: Series B (Statistical Methodology)*, 69(2):243–268, 2007.
- I. Goodfellow, J. Pouget-Abadie, M. Mirza, B. Xu, D. Warde-Farley, S. Ozair, A. Courville, and Y. Bengio. Generative adversarial nets. *Advances in neural information processing systems*, 27, 2014.
- D. Greenberg, M. Nonnenmacher, and J. Macke. Automatic posterior transformation for likelihood-free inference. In K. Chaudhuri and R. Salakhutdinov, editors, *Proceedings of the 36th International Conference on Machine Learning*, volume 97 of *Proceedings of Machine Learning Research*, pages 2404–2414. PMLR, 09–15 Jun 2019. URL <http://proceedings.mlr.press/v97/greenberg19a.html>.

- A. Gretton, K. M. Borgwardt, M. J. Rasch, B. Schölkopf, and A. Smola. A kernel two-sample test. *The Journal of Machine Learning Research*, 13(1):723–773, 2012.
- A. A. Gritsenko, T. Salimans, R. v. d. Berg, J. Snoek, and N. Kalchbrenner. A spectral energy distance for parallel speech synthesis. *arXiv preprint arXiv:2008.01160*, 2020.
- A. Harakeh and S. L. Waslander. Estimating and evaluating regression predictive uncertainty in deep object detectors. In *International Conference on Learning Representations*, 2021. URL <https://openreview.net/forum?id=YLeWtnvKgR7>.
- D. P. Kingma and M. Welling. Auto-encoding variational Bayes. *arXiv preprint arXiv:1312.6114*, 2013.
- J. Lintusaari, M. U. Gutmann, R. Dutta, S. Kaski, and J. Corander. Fundamentals and recent developments in approximate Bayesian computation. *Systematic Biology*, 66(1):e66–e82, 2017. ISSN 1076836X. doi: 10.1093/sysbio/syw077. URL <https://doi.org/10.1093/sysbio/syw077>.
- J.-M. Lueckmann, P. J. Goncalves, G. Bassetto, K. Öcal, M. Nonnenmacher, and J. H. Macke. Flexible statistical inference for mechanistic models of neural dynamics. In *Advances in Neural Information Processing Systems*, pages 1289–1299, 2017.
- J.-M. Lueckmann, G. Bassetto, T. Karaletsos, and J. H. Macke. Likelihood-free inference with emulator networks. In *Symposium on Advances in Approximate Bayesian Inference*, pages 32–53. PMLR, 2019.
- J.-M. Lueckmann, J. Boelts, D. Greenberg, P. Goncalves, and J. Macke. Benchmarking simulation-based inference. In A. Banerjee and K. Fukumizu, editors, *Proceedings of The 24th International Conference on Artificial Intelligence and Statistics*, volume 130 of *Proceedings of Machine Learning Research*, pages 343–351. PMLR, 13–15 Apr 2021.
- M. Mirza and S. Osindero. Conditional generative adversarial nets. *arXiv preprint arXiv:1411.1784*, 2014.
- H. D. Nguyen, J. Arbel, H. Lü, and F. Forbes. Approximate Bayesian computation via the energy statistic. *IEEE Access*, 8:131683–131698, 2020.
- S. Nowozin, B. Cseke, and R. Tomioka. f-GAN: Training generative neural samplers using variational divergence minimization. In *Proceedings of the 30th International Conference on Neural Information Processing Systems*, pages 271–279, 2016.
- L. Pacchiardi, R. Adewoyin, P. Dueben, and R. Dutta. Probabilistic forecasting with conditional generative networks via scoring rule minimization. *arXiv preprint arXiv:2112.08217*, 2022.
- G. Papamakarios and I. Murray. Fast ε -free inference of simulation models with Bayesian conditional density estimation. In *Advances in Neural Information Processing Systems*, pages 1028–1036, 2016.
- G. Papamakarios, D. Sterratt, and I. Murray. Sequential neural likelihood: Fast likelihood-free inference with autoregressive flows. In K. Chaudhuri and M. Sugiyama, editors, *Proceedings of Machine Learning Research*, volume 89 of *Proceedings of Machine Learning Research*, pages 837–848. PMLR, 16–18 Apr 2019. URL <http://proceedings.mlr.press/v89/papamakarios19a.html>.
- G. Papamakarios, E. Nalisnick, D. J. Rezende, S. Mohamed, and B. Lakshminarayanan. Normalizing flows for probabilistic modeling and inference. *Journal of Machine Learning Research*, 22(57):1–64, 2021. URL <http://jmlr.org/papers/v22/19-1028.html>.
- A. Paszke, S. Gross, F. Massa, A. Lerer, J. Bradbury, G. Chanan, T. Killeen, Z. Lin, N. Gimelshein, L. Antiga, A. Desmaison, A. Kopf, E. Yang, Z. DeVito, M. Raison, A. Tejani, S. Chilamkurthy, B. Steiner, L. Fang, J. Bai, and S. Chintala. PyTorch: An imperative style, high-performance deep learning library. In H. Wallach, H. Larochelle, A. Beygelzimer, F. d’Alché Buc, E. Fox,

- and R. Garnett, editors, *Advances in Neural Information Processing Systems 32*, pages 8024–8035. Curran Associates, Inc., 2019.
- L. F. Price, C. C. Drovandi, A. Lee, and D. J. Nott. Bayesian synthetic likelihood. *Journal of Computational and Graphical Statistics*, 27(1):1–11, 2018.
- S. T. Radev, U. K. Mertens, A. Voss, L. Ardizzone, and U. Köthe. BayesFlow: Learning complex stochastic models with invertible neural networks. *IEEE Transactions on Neural Networks and Learning Systems*, 2020.
- P. Ramesh, J.-M. Lueckmann, J. Boelts, Á. Tejero-Cantero, D. S. Greenberg, P. J. Goncalves, and J. H. Macke. GATSBI: Generative adversarial training for simulation-based inference. In *International Conference on Learning Representations*, 2022. URL <https://openreview.net/forum?id=kR1hC6j48Tp>.
- E. Richardson and Y. Weiss. On GANs and GMMs. In *Proceedings of the 32nd International Conference on Neural Information Processing Systems*, pages 5852–5863, 2018.
- M. L. Rizzo and G. J. Székely. Energy distance. *Wiley interdisciplinary reviews: Computational statistics*, 8(1):27–38, 2016.
- S. Talts, M. Betancourt, D. Simpson, A. Vehtari, and A. Gelman. Validating bayesian inference algorithms with simulation-based calibration. *arXiv preprint arXiv:1804.06788*, 2018.

Appendix

A f -GAN

The problem in Eq (2.1) can be obtained as a relaxation of the following one:

$$\arg \min_{\phi} \mathbb{E}_{\mathbf{Y} \sim P} [D_{JS}(\Pi(\cdot|\mathbf{Y})||Q_{\phi}(\cdot|\mathbf{Y}))],$$

where D_{JS} is the Jensen-Shannon divergence. The objective in the above problem is 0 if and only if $\Pi(\cdot|\mathbf{y}) = Q_{\phi}(\cdot|\mathbf{y})$ for each $\mathbf{y} : p(\mathbf{y}) > 0$. We report here a more general result by considering a class of divergences known as f -divergences, to which the Jensen-Shannon one belongs. We follow Nowozin et al. [2016] in doing so⁶.

By discarding temporarily dependence on \mathbf{Y} , an f -divergence is defined as:

$$D_f(P||Q_{\phi}) = \int q_{\phi}(\boldsymbol{\theta}) f\left(\frac{p(\boldsymbol{\theta})}{q_{\phi}(\boldsymbol{\theta})}\right) d\mu(\boldsymbol{\theta}),$$

where $f : \mathbb{R}_+ \rightarrow \mathbb{R}$ is a convex, lower-semicontinuous function for which $f(1) = 0$, and where q_{ϕ} and p are densities of Q_{ϕ} and P with respect to a base measure μ . We want now to fix ϕ via:

$$\arg \min_{\phi} D_f(P||Q_{\phi}). \tag{8}$$

Let now dom_f denote the domain of f . By exploiting the Fenchel conjugate $f^*(t) = \sup_{u \in \text{dom}_f} \{ut - f(u)\}$, Nowozin et al., 2016 obtain the following variational lower bound:

$$D_f(P||Q_{\phi}) \geq \sup_{c \in \mathcal{C}} \left(\mathbb{E}_{\boldsymbol{\theta} \sim P} c(\boldsymbol{\theta}) - \mathbb{E}_{\tilde{\boldsymbol{\theta}} \sim Q_{\phi}} f^*(c(\tilde{\boldsymbol{\theta}})) \right),$$

which holds for any set of functions \mathcal{C} from \mathcal{Y} to dom_{f^*} . By considering a parametric set of functions $\mathcal{C} = \{c_{\psi} : \mathcal{Y} \rightarrow \text{dom}_{f^*}, \psi \in \Psi\}$, a surrogate to the problem in Eq. (A) becomes:

$$\min_{\phi} \max_{\psi} \left(\mathbb{E}_{\boldsymbol{\theta} \sim P} c_{\psi}(\boldsymbol{\theta}) - \mathbb{E}_{\tilde{\boldsymbol{\theta}} \sim Q_{\phi}} f^*(c_{\psi}(\tilde{\boldsymbol{\theta}})) \right).$$

By re-introducing the dependence on \mathbf{Y} , the above generalizes to:

$$\min_{\phi} \max_{\psi} \mathbb{E}_{\mathbf{Y} \sim P} \left(\left(\mathbb{E}_{\boldsymbol{\theta} \sim P(\cdot|\mathbf{Y})} c_{\psi}(\boldsymbol{\theta}, \mathbf{Y}) - \mathbb{E}_{\tilde{\boldsymbol{\theta}} \sim Q_{\phi}(\cdot|\mathbf{Y})} f^*(c_{\psi}(\tilde{\boldsymbol{\theta}}, \mathbf{Y})) \right) \right), \tag{10}$$

where now the function c_{ψ} also depends on the value of \mathbf{Y} .

In practice, c_{ψ} is parametrized by a Neural Network. To solve the problem in Eq. (A), people usually employ alternating optimization over ϕ and ψ by following stochastic gradients; this technique is called f -GAN. With a finite number of steps over ψ , this leads to biased gradient estimates for ϕ . In Algorithm 1, we show a single epoch (i.e., a loop on the full training dataset) of conditional f -GAN training; for simplicity, we consider here using a single pair $(\boldsymbol{\theta}_i, \mathbf{y}_i)$ to estimate the expectations in Eq. (A) (i.e., the batch size is 1), but using a larger number of samples is possible. Notice how in Algorithm 1 we update the critic once every generator update; however, multiple critic updates can be done at each generator update.

B Unbiased gradient estimates

We discuss here how we can get unbiased gradient estimates for the Scoring Rule training objective in Eq. (3.1) with respect to the parameters of the generative network ϕ .

In order to do that, we first discuss how to obtain unbiased estimates of the SRs we use across this work. Then, we show how those allow to obtain unbiased gradient estimates. The steps we follow are the same as in Pacchiardi et al. [2022] for the setting of probabilistic forecasting.

⁶An analogous procedure allows to obtain a tractable training objective for the 1-Wasserstein distance as well Arjovsky et al. [2017]

Algorithm 1 Single epoch conditional f -GAN training.

Require: Parametric map g_ϕ , critic network c_ψ , learning rates ϵ, γ .

for each training pair $(\boldsymbol{\theta}_i, \mathbf{y}_i)$ **do**

 Sample $\mathbf{z} \sim P_{\mathbf{z}}$

 Obtain $\tilde{\boldsymbol{\theta}}_i^\phi = g_\phi(\mathbf{z}, \mathbf{y}_i)$

 Set $\psi \leftarrow \psi + \gamma \cdot \nabla_\psi [c_\psi(\boldsymbol{\theta}_i, \mathbf{y}_i) - f^*(c_\psi(\tilde{\boldsymbol{\theta}}_i^\phi, \mathbf{y}_i))]$

 Set $\phi \leftarrow \phi - \epsilon \cdot \nabla_\phi [-f^*(c_\psi(\tilde{\boldsymbol{\theta}}_i^\phi, \mathbf{y}_i))]$

end for

B.1 Unbiased scoring rule estimates

Assume we have draws $\tilde{\mathbf{x}}_j \sim P, j = 1, \dots, m$.

Energy Score An unbiased estimate of the energy score can be obtained by unbiasedly estimating the expectations in $S_E^{(\beta)}(P, \mathbf{x})$ in Eq. (3.2):

$$\hat{S}_E^{(\beta)}(P, \mathbf{x}) = \frac{2}{m} \sum_{j=1}^m \|\tilde{\mathbf{x}}_j - \mathbf{x}\|_2^\beta - \frac{1}{m(m-1)} \sum_{\substack{j,k=1 \\ k \neq j}}^m \|\tilde{\mathbf{x}}_j - \tilde{\mathbf{x}}_k\|_2^\beta.$$

Kernel Score Similarly to the energy score, we obtain an unbiased estimate of $S_k(P, \mathbf{x})$ in Eq. (3.2) by:

$$\hat{S}_k(P, \mathbf{x}) = \frac{1}{m(m-1)} \sum_{\substack{j,k=1 \\ k \neq j}}^m k(\tilde{\mathbf{x}}_j, \tilde{\mathbf{x}}_k) - \frac{2}{m} \sum_{j=1}^m k(\tilde{\mathbf{x}}_j, \mathbf{x}).$$

Sum of SRs When adding multiple SRs, an unbiased gradient of the sum can be obtained by adding unbiased estimates of the two addends.

B.2 Unbiased estimate of the training objective

Recall now we want to solve:

$$\hat{\phi} := \arg \min_{\phi} J(\phi), \quad J(\phi) = \frac{1}{n} \sum_{i=1}^n S(Q_\phi(\cdot | \mathbf{y}_i), \boldsymbol{\theta}_i) \quad (11)$$

In order to do this, we exploit Stochastic Gradient Descent (SGD), which requires unbiased estimates of $J(\phi)$. Notice how, for all the Scoring Rules used across this work, as well as any weighted sum of those, we can write: $S(P, \mathbf{x}) = \mathbb{E}_{\tilde{\mathbf{X}}, \tilde{\mathbf{X}}' \sim P} [h(\tilde{\mathbf{X}}, \tilde{\mathbf{X}}', \mathbf{x})]$ for some function h ; namely, the SR is defined through an expectation over (possibly multiple) samples from P . That is the form exploited in Appendix B.1 to obtain unbiased SR estimates.

Now, we will use this fact to obtain unbiased estimates for the objective in Eq. (B.2).

$$J(\phi) = \frac{1}{n} \sum_{i=1}^n \mathbb{E}_{\tilde{\boldsymbol{\theta}}, \tilde{\boldsymbol{\theta}}' \sim Q_\phi(\cdot | \mathbf{y}_i)} [h(\tilde{\boldsymbol{\theta}}, \tilde{\boldsymbol{\theta}}', \boldsymbol{\theta}_i)] = \frac{1}{n} \sum_{i=1}^n \mathbb{E}_{\mathbf{Z}, \mathbf{Z}' \sim P_{\mathbf{z}}} [h(g_\phi(\mathbf{Z}, \mathbf{y}_i), g_\phi(\mathbf{Z}', \mathbf{y}_i), \boldsymbol{\theta}_i)],$$

where we used the fact that Q_ϕ is the distribution induced by a generative network with transformation g_ϕ ; this is called the reparametrization trick Kingma and Welling [2013]. Now:

$$\begin{aligned} \nabla_\phi J(\phi) &= \nabla_\phi \frac{1}{n} \sum_{i=1}^n \mathbb{E}_{\mathbf{Z}, \mathbf{Z}' \sim P_{\mathbf{z}}} [h(g_\phi(\mathbf{Z}, \mathbf{y}_i), g_\phi(\mathbf{Z}', \mathbf{y}_i), \boldsymbol{\theta}_i)] \\ &= \frac{1}{n} \sum_{i=1}^n \mathbb{E}_{\mathbf{Z}, \mathbf{Z}' \sim P_{\mathbf{z}}} [\nabla_\phi h(g_\phi(\mathbf{Z}, \mathbf{y}_i), g_\phi(\mathbf{Z}', \mathbf{y}_i), \boldsymbol{\theta}_i)]. \end{aligned}$$

In the latter equality, the exchange between expectation and gradient is not a trivial step, due to the non-differentiability of functions (such as ReLU) used in g_ϕ . Luckily, Theorem 5 in Bińkowski et al. [2018] proved that to be valid almost surely with respect to a measure on the space Φ to which neural network weights ϕ belong, under mild conditions on the NN architecture.

We can now easily obtain an unbiased estimate of the above using samples $\mathbf{z}_{i,j} \sim Q, j = 1, \dots, m$, for each $i \in \{1, \dots, n\}$. Additionally, Stochastic Gradient Descent usually considers a small batch of training samples at each step, obtained by taking a random subset (or batch) $\mathcal{B} \subseteq \{1, 2, \dots, n\}$. Therefore, the following unbiased estimate of $\nabla_\phi J(\phi)$ can be obtained:

$$\widehat{\nabla_\phi J(\phi)} = \frac{1}{|\mathcal{B}|} \sum_{i \in \mathcal{B}} \frac{1}{m(m-1)} \sum_{\substack{j,k=1 \\ j \neq k}}^m \nabla_\phi h(g_\phi(\mathbf{z}_{i,j}; \mathbf{y}_i), g_\phi(\mathbf{z}_{i,k}; \mathbf{y}_i), \boldsymbol{\theta}_i).$$

In practice, the above is obtained by computing the gradient of the following unbiased estimate of $J(\phi)$ via autodifferentiation libraries (see for instance Paszke et al., 2019):

$$\hat{J}(\phi) = \frac{1}{|\mathcal{B}|} \sum_{i \in \mathcal{B}} \frac{1}{m(m-1)} \sum_{\substack{j,k=1 \\ j \neq k}}^m h(g_\phi(\mathbf{z}_{i,j}; \mathbf{y}_i), g_\phi(\mathbf{z}_{i,k}; \mathbf{y}_i), \boldsymbol{\theta}_i).$$

In Algorithm 2, we train a generative network for a single epoch using a scoring rule S for which unbiased estimators can be obtained by using more than one sample from Q_ϕ . Compare it with the adversarial approach reported in Algorithm 1; in the SR approach, multiple samples from the generative networks are required at each step ($m > 1$), while a unique one is enough for the adversarial approach. Conversely, however, the SR approach does not require an additional critic network and learning rate γ and is simpler and quicker to train (see the results in Sec. 4 and Pacchiardi et al., 2022 for more details). As in Algorithm 1, we use a single pair $(\boldsymbol{\theta}_i, \mathbf{y}_i)$ to estimate the gradient.

Algorithm 2 Single epoch generative-SR training.

Require: Parametric map g_ϕ , SR S , learning rate ϵ .

for each training pair $(\boldsymbol{\theta}_i, \mathbf{y}_i)$ **do**

 Sample **multiple** $\mathbf{z}_1, \dots, \mathbf{z}_m$

 Obtain $\tilde{\boldsymbol{\theta}}_{i,j}^\phi = g_\phi(\mathbf{z}_j, \mathbf{y}_i)$

 Obtain unbiased estimate $\hat{S}(Q_\phi(\cdot | \mathbf{y}_i), \boldsymbol{\theta}_i)$ from $\tilde{\boldsymbol{\theta}}_{i,j}^\phi$

 Set $\phi \leftarrow \phi - \epsilon \cdot \nabla_\phi \hat{S}(Q_\phi(\cdot | \mathbf{y}_i), \boldsymbol{\theta}_i)$

end for

C Details on performance measures

We review here the measures of performance used in the empirical studies. We follow Radev et al. [2020] in defining these measures; we report them here for ease of reference. All these metrics are for univariate $\boldsymbol{\theta}$; when handling multivariate $\boldsymbol{\theta}$, we therefore compute them on each dimension separately and report the average.

C.1 Deterministic performance measures

We discuss two measures of performance of a deterministic forecast $\hat{\boldsymbol{\theta}}_i$ for a realization $\boldsymbol{\theta}_i$; across our work, we take $\hat{\boldsymbol{\theta}}_i$ to be the mean of the (univariate) probability distribution $Q_\phi(\cdot | \mathbf{y}_i)$.

C.1.1 RMSE

We first introduce the Root Mean-Square Error (RMSE) as:

$$\text{RMSE} = \sqrt{\frac{1}{n} \sum_{i=1}^n (\hat{\boldsymbol{\theta}}_i - \boldsymbol{\theta}_i)^2},$$

where we consider here for simplicity $i = 1, \dots, n$. From the above, we obtain the Normalized RMSE (NRMSE) as:

$$\text{NRMSE} = \frac{\text{RMSE}}{\max_i\{\boldsymbol{\theta}_i\} - \min_i\{\boldsymbol{\theta}_i\}}.$$

NRMSE = 0 implies $\hat{\boldsymbol{\theta}}_i = \boldsymbol{\theta}_i$ for all i 's. NRMSE $\in [0, 1]$ and allows to compare performance over different tasks. Notice however that, when $\max_i\{\boldsymbol{\theta}_i\} = \min_i\{\boldsymbol{\theta}_i\}$, NRMSE diverges; in that case, we consider the un-normalized RMSE.

C.1.2 Coefficient of determination

The coefficient of determination R^2 measures how much of the variance in $\{\boldsymbol{\theta}_i\}_{i=1}^n$ is explained by $\{\hat{\boldsymbol{\theta}}_i\}_{i=1}^n$. Specifically, it is given by:

$$R^2 = 1 - \frac{\sum_{i=1}^n (\boldsymbol{\theta}_i - \hat{\boldsymbol{\theta}}_i)^2}{\sum_{i=1}^n (\boldsymbol{\theta}_i - \bar{\boldsymbol{\theta}})^2},$$

where $\bar{\boldsymbol{\theta}} = \frac{1}{n} \sum_{i=1}^n \boldsymbol{\theta}_i$. $R^2 \leq 1$ and $R^2 = 1 \implies \hat{\boldsymbol{\theta}}_i = \boldsymbol{\theta}_i$ for all i 's.

C.2 Calibration measures

We review here two measures of calibration of a probabilistic forecast. Both measures consider the univariate marginals of the approximate posterior distribution $Q_\phi(\cdot|\mathbf{y}_i)$; for component l , let us denote that by $Q_{\phi,l}(\cdot|\mathbf{y}_i)$.

C.2.1 Calibration error

The calibration error Radev et al. [2020] quantifies how well the credible intervals of approximate posterior $Q_{\phi,l}(\cdot|\mathbf{y}_i)$ match the distribution of $\theta_{i,l}$. Specifically, let $\alpha(l)$ be the proportion of times the verification $\theta_{i,l}$ falls into an α -credible interval of $Q_{\phi,l}(\cdot|\mathbf{y}_i)$, computed over all values of i . If the marginal forecast distribution is perfectly calibrated for component l , $\alpha(l) = \alpha$ for all values of $\alpha \in (0, 1)$.

We define therefore the calibration error as the median of $|\alpha(l) - \alpha|$ over 100 equally spaced values of $\alpha \in (0, 1)$. Therefore, the calibration error is a value between 0 and 1, where 0 denotes perfect calibration.

In practice, the credible intervals of the predictive are estimated using a set of samples from $Q_\phi(\cdot|\mathbf{y}_i)$.

C.2.2 Simulation-Based Calibration (SBC)

SBC Talts et al. [2018] tests a self-consistency property of the Bayesian posterior in a posterior approximation. In fact, the Bayesian posterior satisfies the following equality:

$$\pi(\boldsymbol{\theta}) = \int p(\boldsymbol{\theta}, \tilde{\boldsymbol{\theta}}, \tilde{\mathbf{y}}) d\tilde{\mathbf{y}} d\tilde{\boldsymbol{\theta}} = \int p(\boldsymbol{\theta}, \tilde{\mathbf{y}} | \tilde{\boldsymbol{\theta}}) \pi(\tilde{\boldsymbol{\theta}}) d\tilde{\mathbf{y}} d\tilde{\boldsymbol{\theta}} = \int \pi(\boldsymbol{\theta} | \tilde{\mathbf{y}}) p(\tilde{\mathbf{y}} | \tilde{\boldsymbol{\theta}}) \pi(\tilde{\boldsymbol{\theta}}) d\tilde{\mathbf{y}} d\tilde{\boldsymbol{\theta}} \quad (12)$$

in practice, this means that, if you sample from the prior $\tilde{\boldsymbol{\theta}} \sim \pi$, use that to generate a sample from the likelihood $\tilde{\mathbf{y}} \sim p(\cdot|\tilde{\boldsymbol{\theta}})$ and use the latter in turn to generate a posterior sample $\boldsymbol{\theta} \sim \pi(\cdot|\tilde{\mathbf{y}})$, $\boldsymbol{\theta}$ is distributed according to the prior $\pi(\boldsymbol{\theta})$. If you repeat the same procedure by sampling $\boldsymbol{\theta}$ from an *approximate* posterior, say $\boldsymbol{\theta} \sim Q_\phi(\cdot|\tilde{\mathbf{y}})$, then $\boldsymbol{\theta} \sim \pi$ is a necessary condition for $q_\phi(\cdot|\mathbf{y}) = \pi(\cdot|\mathbf{y})$, i.e. for the approximate posterior to be exact. Notice however how this is *not* a sufficient condition: the equality can be satisfied even if $q_\phi(\cdot|\mathbf{y})$ is different from the posterior (it is in fact trivially satisfied $q_\phi(\cdot|\mathbf{y}) = \pi$, i.e. when the approximate posterior corresponds to the prior).

A way to empirically test the above property involves, for a given prior sample $\tilde{\boldsymbol{\theta}}$, drawing from the likelihood multiple times $\mathbf{y}_i \sim p(\cdot|\tilde{\boldsymbol{\theta}})$, $i = 1, \dots, N$ and, for each of these, obtaining a single approximate

posterior sample $\theta_i \sim q_\phi(\cdot|\mathbf{y}_i)$. Given these, you compute the rank of $\tilde{\theta}$: $r = \sum_{i=1}^N \mathbf{1}_{[\theta_i < \tilde{\theta}]}$ (this only makes sense if θ is univariate; otherwise, you compute the rank independently for each dimension of θ). If θ_i 's were effectively distributed from the prior, r is a uniform random variable on $\{1, 2, \dots, N\}$. Therefore, by repeating this procedure for different prior samples $\tilde{\theta}$ and visualizing the distribution of the resulting r 's (for instance via an histogram or by plotting the CDF) gives an indication of whether an equivalence such as Eq. (C.2.2) is satisfied for q_ϕ . See Algorithm 2 in Radev et al. [2020] for a precise description of this procedure, which goes under the name of Simulation-Based Calibration. This is closely related to the concept of probabilistic calibration and rank histogram in the framework of probabilistic forecasting [Gneiting et al., 2007].

D Experimental details

Precise configuration details can be found in the code accompanying the paper.

D.1 Benchmark models

Except for the details reported in the main body of the paper, the training configuration for the two benchmark models is the same as in Ramesh et al. [2022]; of course, some hyperparameter values for the GAN training routine do not apply to the SR one (for instance, all the hyperparameters related to the discriminator).

D.2 Shallow Water Model

We train all methods for at most 40k epochs on 100k training samples. For the SR method, we tried both $m = 3$ and $m = 10$, with the latter resulting in improved performance; all results reported across the paper refer therefore to $m = 10$.

GAN used a batch size of 125 (as in Ramesh et al., 2022), while the SR methods used a batch size of 60 (otherwise GPU memory overflow occurs).

Recall that the parameters $\theta \in \mathbb{R}^{100}$ are disposed along a 1D uniform grid. When using the patched SR configuration, we consider patches of size `patch_size` disposed at a distance `patch_step` one from the other. The number of patches is therefore

$$\text{n_patches} = (100 - \text{patch_size})/\text{patch_step} + 1.$$

We used therefore the following patched SR configurations on the 1D grid:

1. `patch_size = 10` and `patch_step = 5`, which results in `n_patches = 19`.
2. `patch_size = 20` and `patch_step = 10`, which results in `n_patches = 9`.

The patched SR is added to the overall score over the full parameter space.

The training time (per epoch) is roughly constant in the un-patched and the two different patched configurations.

D.3 Camera Model

We train all methods for at most 10k epochs on 800k training samples. For the SR method, we tried both $m = 3$ and $m = 10$, with the latter resulting in improved performance.

Both SR and GAN methods used a batch size of 800 as in Ramesh et al. [2022].

Here, the parameters θ is on a 28×28 square grid. When using the patched SR configuration, we consider patches of size `patch_size` \times `patch_size` disposed at a distance `patch_step` one from the other in both spatial dimensions. the number of patches is obtained as

$$\text{n_patches} = [(28 - \text{patch_size})/\text{patch_step} + 1]^2.$$

We used therefore the following patched SR configurations on the 2D grid:

1. `patch_size = 14` and `patch_step = 7`, which results in `n_patches = 9`.
2. `patch_size = 8` and `patch_step = 5`, which results in `n_patches = 25`.

The patched SR is added to the overall score over the full parameter space.

The training time (per epoch) is roughly constant in the un-patched and the two different patched configurations.

E Additional experimental results

E.1 SLCP

In Figure 5, we report posterior samples obtained with the Energy Score with $m = 20$ and compare them with samples from the reference posterior. In Figure 6, we report Simulation-Based Calibration results (see Appendix C.2.2): for each dimension of θ , each histogram represents the distribution of the rank of the true parameter value in a set of samples from the approximate posterior. We show that for GAN and for the Energy Score with $m = 20$.

Tables 5, 6, 7, 8, 9 and 10 report the different performance metrics, the runtime and the early stopping epoch for all methods (columns) and all number of training samples (rows); for Energy and Kernel Score, the number in the column header denotes the number of draws from the generative network during training for each \mathbf{y}_i in the training batch.

Table 5: SLCP: classification-based two-sample test (C2ST).

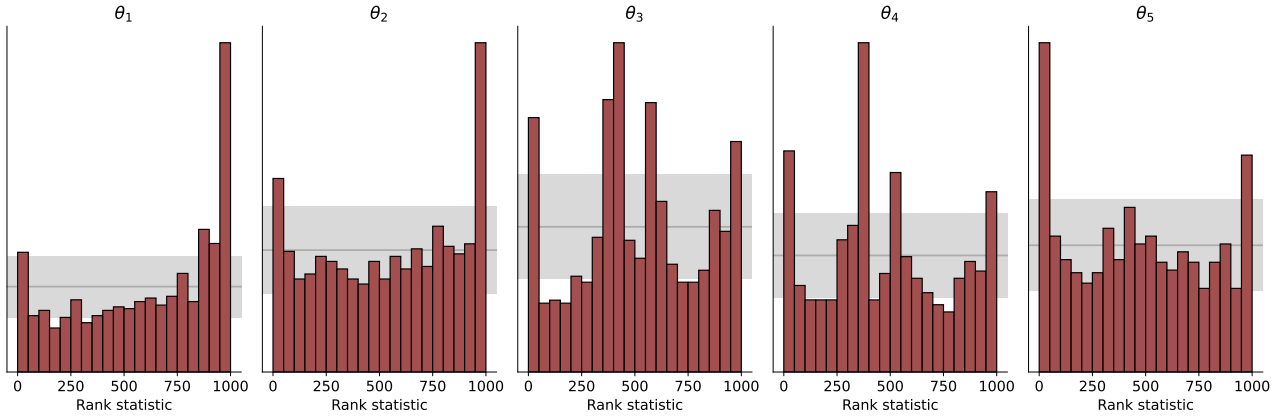
	GAN	Energy 3	Energy 5	Energy 10	Energy 20	Kernel 3	Kernel 5	Kernel 10	Kernel 20
1000	0.97 ± 0.02	0.99 ± 0.01	0.99 ± 0.01	0.99 ± 0.00	0.99 ± 0.01	1.00 ± 0.01	0.99 ± 0.01	0.99 ± 0.01	0.99 ± 0.01
10000	0.94 ± 0.03	0.98 ± 0.01	0.97 ± 0.01	0.98 ± 0.01	0.98 ± 0.01	0.99 ± 0.01	0.99 ± 0.01	0.99 ± 0.01	0.99 ± 0.01
100000	0.92 ± 0.03	0.97 ± 0.01	0.97 ± 0.02	0.96 ± 0.02	0.95 ± 0.02	0.98 ± 0.01	0.98 ± 0.01	0.98 ± 0.01	0.98 ± 0.01

Table 6: SLCP: NRMSE.

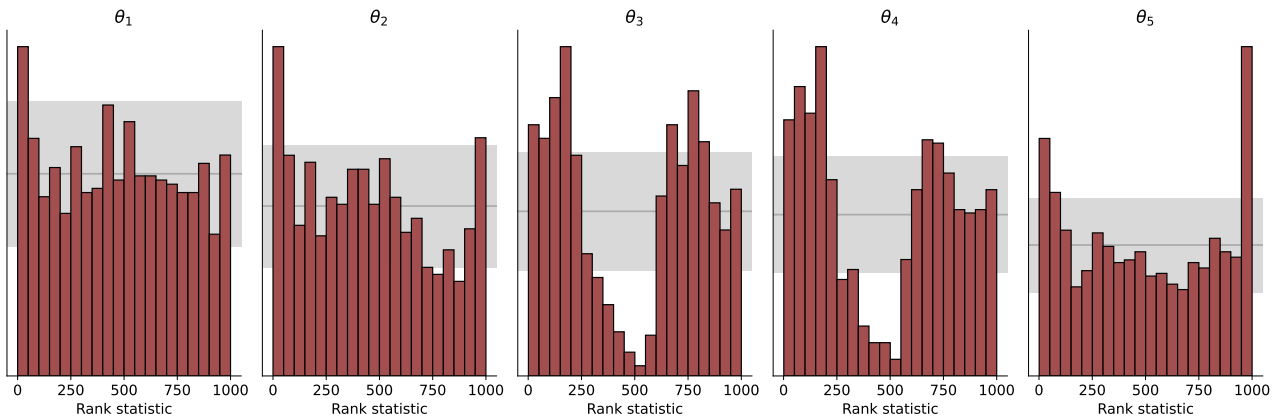
	GAN	Energy 3	Energy 5	Energy 10	Energy 20	Kernel 3	Kernel 5	Kernel 10	Kernel 20
1000	0.24 ± 0.05	0.25 ± 0.05	0.25 ± 0.05	0.25 ± 0.05	0.25 ± 0.06	0.25 ± 0.05	0.25 ± 0.05	0.25 ± 0.05	0.25 ± 0.05
10000	0.23 ± 0.05	0.23 ± 0.05	0.23 ± 0.05	0.23 ± 0.05	0.23 ± 0.05	0.23 ± 0.05	0.23 ± 0.05	0.23 ± 0.05	0.23 ± 0.05
100000	0.23 ± 0.05	0.22 ± 0.05	0.22 ± 0.06	0.22 ± 0.06	0.22 ± 0.06	0.22 ± 0.06	0.22 ± 0.06	0.22 ± 0.05	0.22 ± 0.06

Table 7: SLCP: calibration error.

	GAN	Energy 3	Energy 5	Energy 10	Energy 20	Kernel 3	Kernel 5	Kernel 10	Kernel 20
1000	0.13 ± 0.05	0.19 ± 0.07	0.20 ± 0.05	0.20 ± 0.05	0.22 ± 0.07	0.24 ± 0.09	0.23 ± 0.10	0.24 ± 0.08	0.24 ± 0.08
10000	0.08 ± 0.03	0.11 ± 0.05	0.10 ± 0.05	0.12 ± 0.07	0.10 ± 0.07	0.15 ± 0.10	0.13 ± 0.09	0.14 ± 0.10	0.16 ± 0.10
100000	0.06 ± 0.03	0.08 ± 0.07	0.08 ± 0.04	0.07 ± 0.05	0.07 ± 0.04	0.13 ± 0.11	0.13 ± 0.10	0.12 ± 0.08	0.13 ± 0.10



(a) GAN



(b) Energy Score, $m = 20$

Figure 6: SLCP: Simulation-Based Calibration results represented as rank histograms; for each dimension of θ , each histogram represents the distribution of the rank of the true parameter value in a set of samples from the approximate posterior. If the approximate posterior is calibrated, histogram bars should be in the grey region with 99% probability.

Table 8: SLCP: R^2 .

	GAN	Energy 3	Energy 5	Energy 10	Energy 20	Kernel 3	Kernel 5	Kernel 10	Kernel 20
1000	0.25 ± 0.29	0.24 ± 0.30	0.22 ± 0.30	0.25 ± 0.31	0.18 ± 0.35	0.22 ± 0.30	0.22 ± 0.30	0.24 ± 0.30	0.23 ± 0.31
10000	0.35 ± 0.30	0.35 ± 0.30	0.35 ± 0.30	0.35 ± 0.30	0.34 ± 0.31	0.35 ± 0.29	0.35 ± 0.30	0.34 ± 0.30	0.34 ± 0.30
100000	0.35 ± 0.30	0.36 ± 0.30	0.37 ± 0.30	0.38 ± 0.32	0.38 ± 0.32	0.37 ± 0.31	0.36 ± 0.31	0.36 ± 0.30	0.37 ± 0.31

Table 9: SLCP: runtime in seconds; recall that GAN was trained on GPU while the SR methods were trained on a single CPU.

	GAN	Energy 3	Energy 5	Energy 10	Energy 20	Kernel 3	Kernel 5	Kernel 10	Kernel 20
1000	4796	654	692	620	885	515	531	682	1330
10000	9671	651	658	639	720	636	658	655	697
100000	30963	1060	1160	1305	1645	1245	1044	1057	1210

Table 10: SLCP: epoch at which early stopping occurred; the max number of training epochs was 20000.

	GAN	Energy 3	Energy 5	Energy 10	Energy 20	Kernel 3	Kernel 5	Kernel 10	Kernel 20
1000	20000	1000	1000	1000	1100	1100	1000	1000	1000
10000	20000	1100	1000	1100	1100	1100	1100	1000	1000
100000	20000	1000	1200	1500	2100	1600	1100	1000	1200

E.2 Two Moons

In Figure 7, we report posterior samples obtained with the Energy Score with $m = 20$ and compare them with samples from the reference posterior. In Figure 8, we report Simulation-Based Calibration results (see Appendix C.2.2): for each dimension of θ , each histogram represents the distribution of the rank of the true parameter value in a set of samples from the approximate posterior. We show that for GAN and for the Energy Score with $m = 20$.

Tables 11, 12, 13, 14, 15 and 16 report the different performance metrics, the runtime and the early stopping epoch for all methods (columns) and all number of training samples (rows); for Energy and Kernel Score, the number in the column header denotes the number of draws from the generative network during training for each \mathbf{y}_i in the training batch.

Table 11: Two Moonsclassification-based two-sample test (C2ST).

	GAN	Energy 3	Energy 5	Energy 10	Energy 20	Kernel 3	Kernel 5	Kernel 10	Kernel 20
1000	0.85 ± 0.05	0.85 ± 0.06	0.87 ± 0.05	0.85 ± 0.03	0.85 ± 0.04	0.94 ± 0.03	0.94 ± 0.02	0.93 ± 0.03	0.96 ± 0.02
10000	0.81 ± 0.03	0.79 ± 0.04	0.76 ± 0.05	0.76 ± 0.04	0.74 ± 0.07	0.92 ± 0.03	0.93 ± 0.01	0.91 ± 0.03	0.93 ± 0.01
100000	0.82 ± 0.07	0.79 ± 0.03	0.74 ± 0.06	0.73 ± 0.05	0.73 ± 0.04	0.90 ± 0.04	0.92 ± 0.03	0.90 ± 0.02	0.92 ± 0.02

Table 12: Two Moons: NRMSE.

	GAN	Energy 3	Energy 5	Energy 10	Energy 20	Kernel 3	Kernel 5	Kernel 10	Kernel 20
1000	0.20 ± 0.00	0.20 ± 0.00	0.20 ± 0.00	0.20 ± 0.00	0.20 ± 0.00	0.21 ± 0.00	0.21 ± 0.00	0.21 ± 0.00	0.20 ± 0.00
10000	0.20 ± 0.00	0.20 ± 0.00	0.20 ± 0.00	0.20 ± 0.00	0.20 ± 0.00	0.20 ± 0.00	0.20 ± 0.00	0.20 ± 0.00	0.20 ± 0.00
100000	0.20 ± 0.00	0.20 ± 0.00	0.20 ± 0.00	0.20 ± 0.00	0.20 ± 0.00	0.20 ± 0.00	0.20 ± 0.00	0.20 ± 0.00	0.20 ± 0.00

Table 13: Two Moons: calibration error.

	GAN	Energy 3	Energy 5	Energy 10	Energy 20	Kernel 3	Kernel 5	Kernel 10	Kernel 20
1000	0.07 ± 0.01	0.05 ± 0.01	0.09 ± 0.02	0.07 ± 0.01	0.06 ± 0.00	0.08 ± 0.01	0.11 ± 0.00	0.14 ± 0.02	0.12 ± 0.01
10000	0.06 ± 0.01	0.04 ± 0.02	0.03 ± 0.01	0.04 ± 0.03	0.03 ± 0.01	0.04 ± 0.00	0.03 ± 0.01	0.03 ± 0.02	0.03 ± 0.01
100000	0.07 ± 0.02	0.04 ± 0.01	0.03 ± 0.00	0.04 ± 0.02	0.03 ± 0.00	0.04 ± 0.00	0.03 ± 0.01	0.06 ± 0.01	0.03 ± 0.01

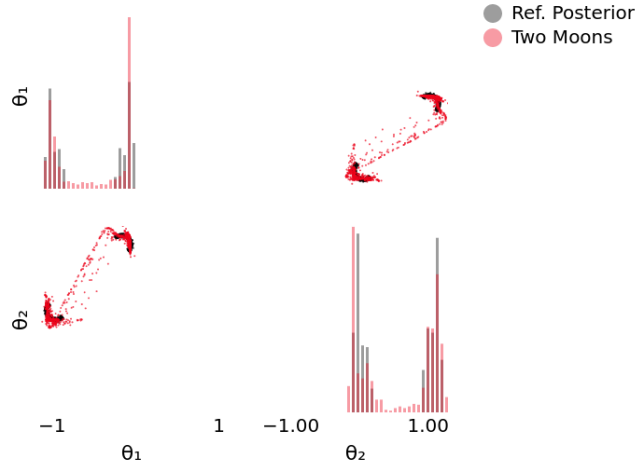


Figure 7: Two Moons: posterior samples for Energy Score trained with $m = 20$ and reference posterior samples. Diagonal panels represent univariate marginals, while off-diagonals represent bivariate marginals. A similar plot for GAN can be found in the supplementary material in Ramesh et al. [2022].

Table 14: Two Moons: R^2 .

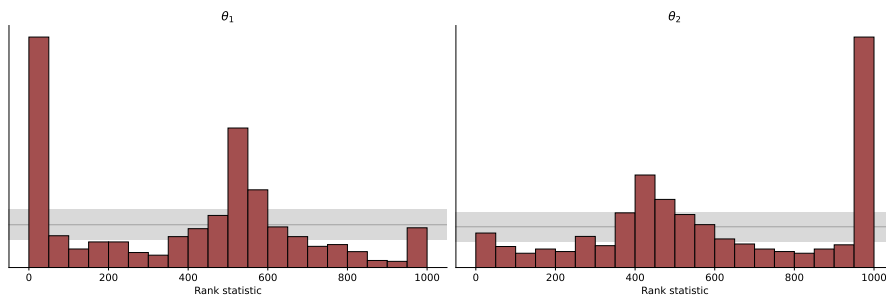
	GAN	Energy 3	Energy 5	Energy 10	Energy 20	Kernel 3	Kernel 5	Kernel 10	Kernel 20
1000	0.50 ± 0.01	0.49 ± 0.01	0.50 ± 0.01	0.50 ± 0.01	0.51 ± 0.01	0.48 ± 0.01	0.49 ± 0.01	0.48 ± 0.01	0.49 ± 0.01
10000	0.49 ± 0.01	0.50 ± 0.01	0.51 ± 0.01	0.51 ± 0.01	0.51 ± 0.01	0.50 ± 0.01	0.50 ± 0.01	0.50 ± 0.01	0.50 ± 0.01
100000	0.51 ± 0.01	0.50 ± 0.01	0.50 ± 0.01	0.50 ± 0.01	0.51 ± 0.01	0.50 ± 0.01	0.51 ± 0.01	0.50 ± 0.01	0.50 ± 0.01

Table 15: Two Moons: runtime in seconds; recall that GAN was trained on GPU while the SR methods were trained on a single CPU.

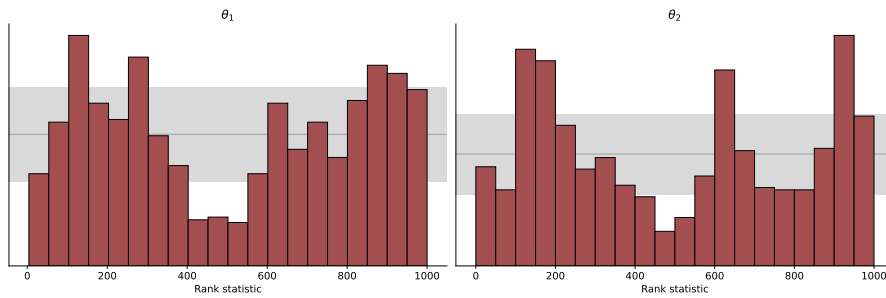
	GAN	Energy 3	Energy 5	Energy 10	Energy 20	Kernel 3	Kernel 5	Kernel 10	Kernel 20
1000	4799	578	690	759	896	585	613	651	852
10000	8163	1775	1917	2415	3228	1708	1883	2329	3267
100000	30232	9266	9388	9903	10805	9283	9479	9859	10902

Table 16: Two Moons: epoch at which early stopping occurred; the max number of training epochs was 20000.

	GAN	Energy 3	Energy 5	Energy 10	Energy 20	Kernel 3	Kernel 5	Kernel 10	Kernel 20
1000	20000	20000	20000	20000	20000	20000	20000	20000	20000
10000	20000	20000	20000	20000	20000	20000	20000	20000	20000
100000	20000	20000	20000	20000	20000	20000	20000	20000	20000



(a) GAN



(b) Energy Score, $m = 20$

Figure 8: Two Moons: Simulation-Based Calibration results represented as rank histograms; for each dimension of θ , each histogram represents the distribution of the rank of the true parameter value in a set of samples from the approximate posterior. If the approximate posterior is calibrated, histogram bars should be in the grey region with 99% probability.

E.3 Shallow Water Model

In Figure 9, we show results, analogously to what done in Figure 2, for all methods. Table 17 reports the different performance metrics, the runtime and the early stopping epoch for all methods. Finally, Figure 10 reports Simulation-Based Calibration results for all SR methods.

Table 17: Shallow Water model: performance metrics, runtime and early stopping epoch for all methods. We do not train GAN from scratch but rather relied on the trained network obtained in Ramesh et al. [2022]. The training time we report here corresponds to what is mentioned in the Ramesh et al. [2022], which used two GPUs for training (with respect to a single one for the SR methods). For the same reason, we do not report the epoch at which GAN training was early stopped.

	RMSE ↓	Cal. Err. ↓	R ² ↑	Runtime (sec)	Early stopping epoch
Energy	0.05 ± 0.01	0.03 ± 0.02	0.87 ± 0.05	51328	10400
Energy patched 10 20	0.05 ± 0.01	0.03 ± 0.02	0.89 ± 0.05	60017	12400
Energy patched 5 10	0.06 ± 0.01	0.03 ± 0.02	0.86 ± 0.06	49626	9600
Kernel	0.06 ± 0.01	0.11 ± 0.05	0.84 ± 0.06	39608	7800
Kernel patched 10 20	0.06 ± 0.01	0.09 ± 0.04	0.86 ± 0.06	47642	9000
Kernel patched 5 10	0.06 ± 0.01	0.09 ± 0.04	0.86 ± 0.06	44590	9200
GAN	0.07 ± 0.01	0.12 ± 0.09	0.78 ± 0.05	≈345600	-

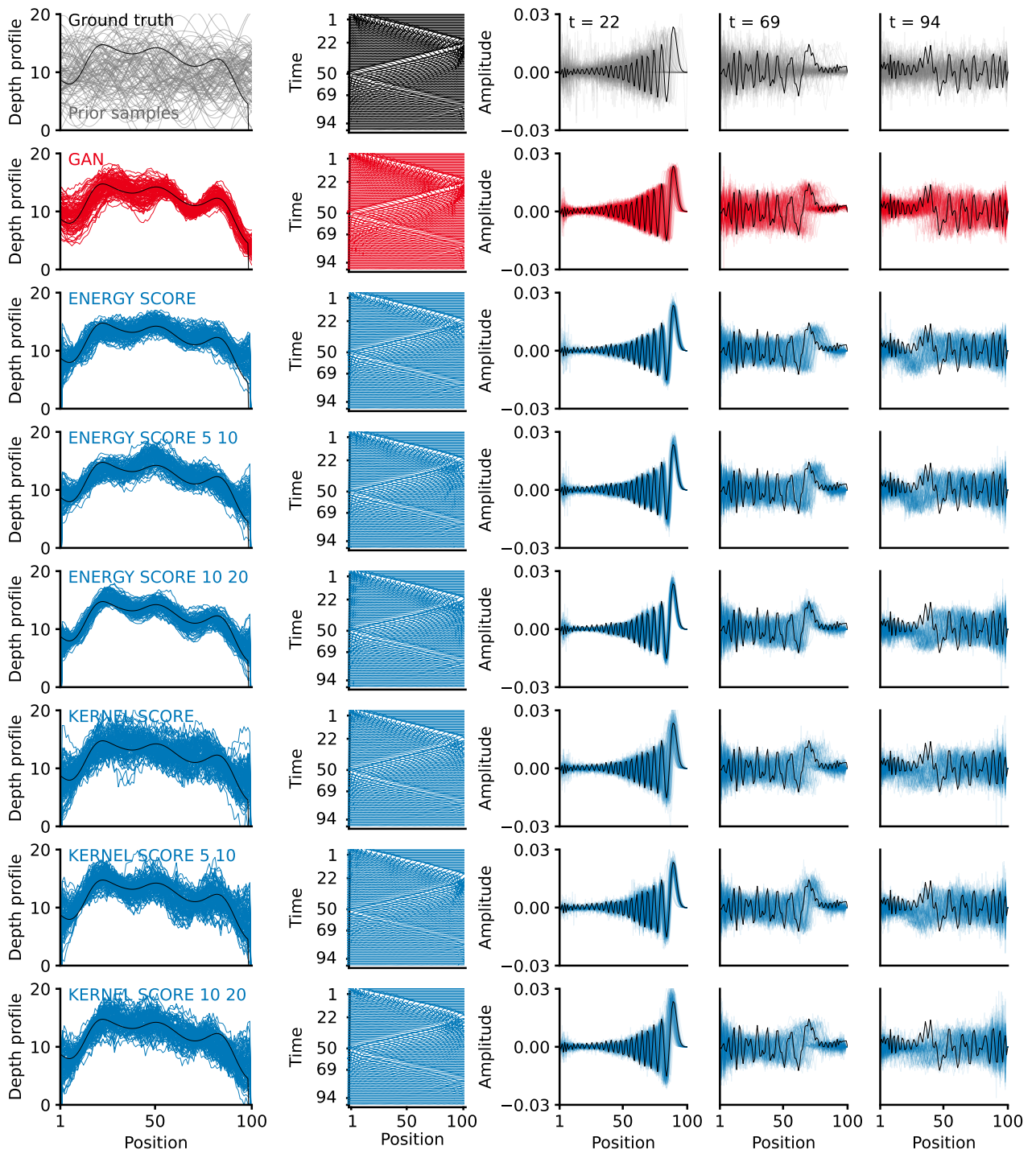
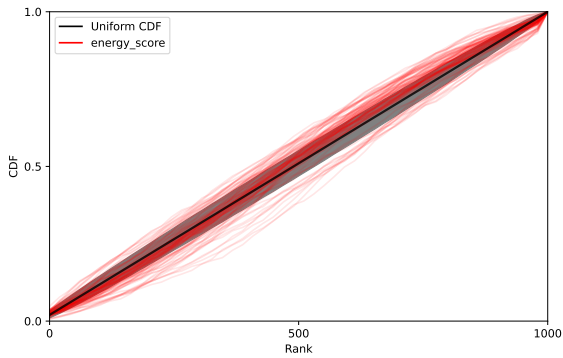
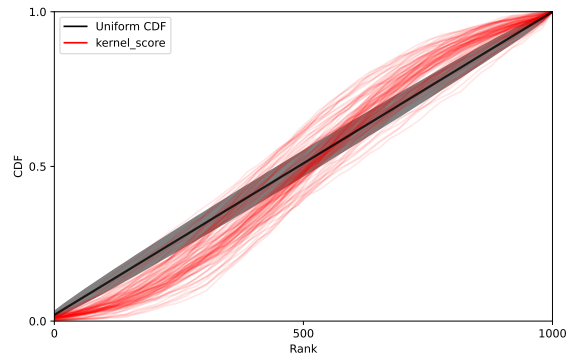


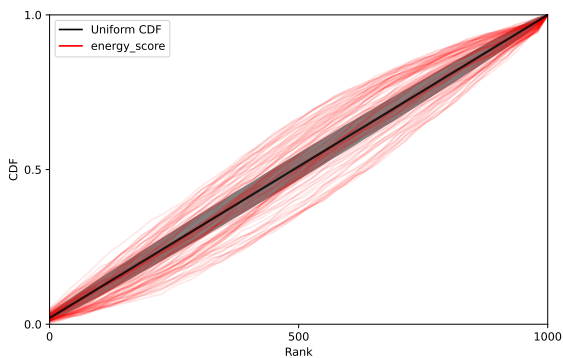
Figure 9: Shallow water model: inference results with all methods. See Figure 2 for description of the different panels.



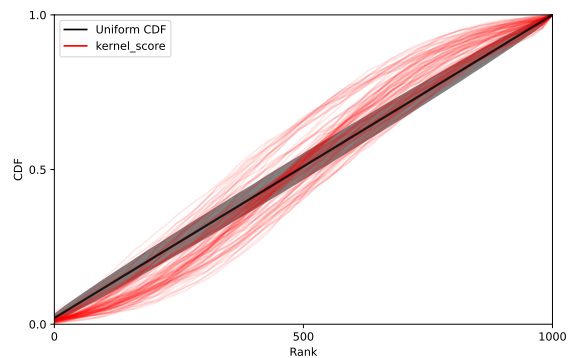
(a) Energy Score



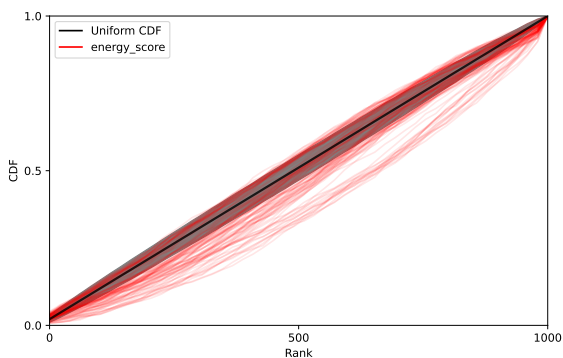
(b) Kernel Score



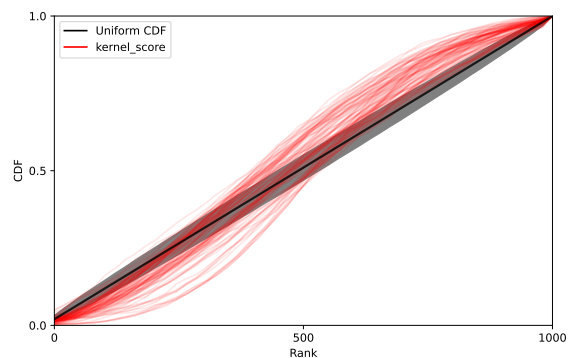
(c) Energy Score patched 5, 10



(d) Kernel Score patched 5, 10



(e) Energy Score patched 10, 20



(f) Kernel Score patched 10, 20

Figure 10: Shallow Water model: Simulation Based Calibration for all SR methods. Each line corresponds to a single dimension of θ and represents the CDF of the rank of the true parameter value with respect to a set of posterior samples. A calibrated posterior implies uniform CDF (diagonal black line, with associated 99% confidence region for that number of samples in gray).

E.4 Camera model

In Figure 11, we show results, analogously to what done in Figure 4, for all methods. Table 18 reports the different performance metrics, the runtime and the early stopping epoch for all methods.

Table 18: Noisy Camera model: performance metrics, runtime and early stopping epoch for all methods.

	RMSE ↓	Cal. Err. ↓	R ² ↑	Runtime (sec)	Early stopping epoch
GAN	0.25 ± 0.19	0.50 ± 0.00	-23.94 ± 366.08	45398	3600
Energy	0.08 ± 0.05	0.36 ± 0.12	-24.39 ± 450.13	24555	4200
Energy patched 5 8	0.06 ± 0.05	0.36 ± 0.12	-2.14 ± 55.86	22633	4000
Energy patched 7 14	0.07 ± 0.05	0.37 ± 0.12	-10.33 ± 227.38	24033	3600
Kernel	0.06 ± 0.05	0.32 ± 0.15	-7.22 ± 164.26	21862	3200
Kernel patched 5 8	0.07 ± 0.05	0.36 ± 0.12	-10.29 ± 222.12	22545	3200
Kernel patched 7 14	0.10 ± 0.06	0.38 ± 0.11	-144.56 ± 2952.80	20605	3600



Figure 11: Noisy Camera model: ground truth and posterior inference with all methods, for a set of observations (each observation corresponds to a column). The first two rows represent the ground-truth values of θ and the corresponding observation y_o . The remaining rows represent mean and Standard Deviation (SD) for all methods.